Pathogen effector-triggered aggregation of TIR-1/SARM1 on lysosome-related organelles activates intestinal immunity

Samantha Y. Tse-Kang,[1] Khursheed A. Wani,[1] Nicholas D. Peterson,[1] Amanda Page,[1] Read Pukkila-Worley[1,2,*]

[1]Program in Innate Immunity, Division of Infectious Diseases and Immunology, Department of Medicine, University of Massachusetts Chan Medical School, Worcester, MA 01655, United States of America, [2]Lead contact

*Correspondence may be addressed to Read Pukkila-Worley (Read.Pukkila-Worley@umassmed.edu, @RPWlab)

SUMMARY

Mechanisms of pathogen recognition in barrier tissues, which interface with both commensal and virulent bacteria, are critical for health and not fully understood. Here, we discovered a central role for lysosome-related organelles in innate immune sensing and p38 innate immune activation in intestinal epithelial cells, which enables the nematode *C. elegans* to survey for the effects of a bacterial pathogen on the host to activate protective anti-pathogen defenses. We showed that the conserved immune signaling regulator TIR-1/SARM1 is expressed on the membranes of lysosome-related organelles. Pyocyanin, a virulence effector secreted by *Pseudomonas aeruginosa,* alkalinized and collapsed lysosome-related organelles, triggering TIR-1/SARM1 multimerization to activate the p38 innate immune pathway. Thus, pathogen effector-mediated collapse of lysosome-related organelles is an initiating event of innate immune sensing and p38 activation, which allows *C. elegans* to identify a pathogen through its effects on host physiology.

KEYWORDS

effector-triggered immunity, lysosome-related organelles, intestinal immunity, TIR-1/SARM1, *Pseudomonas aeruginosa*, *Caenorhabditis elegans,* phenazines

INTRODUCTION

Host cells within barrier tissues and professional immune cells encode receptors that activate protective innate immune signaling pathways upon recognition of structural features of microbes. Surveillance of such Pathogen (or Microbe)-Associated Molecular Patterns (PAMPs/MAMPs), also called Pattern Recognition, is particularly effective at detecting pathogens in normally sterile environments, such as in the bloodstream or meninges. However, PAMPs/MAMPs are not exclusively expressed on harmful microbes, and host cells within barrier tissues, which interface with both commensal and virulent microorganisms, must use other strategies to identify infectious pathogens. For example, both animals and plants have evolved mechanisms to recognize the effects of pathogen-generated virulence effectors on the host. Such mechanisms are often referred to collectively as effector-triggered immunity and are among the most primordial forms of pathogen detection.[1-3] Unlike PAMPs/MAMPs, these so-called "patterns of pathogenesis" specifically indicate the presence of disease-inducing organisms. Since their discovery, mechanisms of effector-triggered immunity have been identified across kingdoms, including in humans, *Drosophila melanogaster,* and *Caenorhabditis elegans.*[1-3]

The nematode *C. elegans* is a particularly useful model for the characterization of bacterial patterns of pathogenesis.[4-6] Nematodes live in microbe-rich habitats and consume bacteria for nutrition. *C. elegans* are therefore constantly in the presence of PAMPs/MAMPs and have lost canonical mechanisms of bacterial pattern recognition during evolution.[4,5,7] Instead, *C. elegans* has evolved strategies to survey patterns of pathogenesis, rather than structural features of bacteria, to distinguish infectious pathogens from its bacterial food. For example, we previously discovered that *C. elegans* uses a non-canonical pattern recognition system to intercept metabolite-based signals of bacterial growth and virulence to evaluate the threat posed by pathogenic bacteria.[8] We found that a *C. elegans* nuclear hormone receptor (NHR-86) binds

phenazine-1-carboxamide (PCN), a virulence effector produced by the bacterial pathogen *Pseudomonas aeruginosa,* and directly activates innate immune defenses.[8] Additionally, pathogen-induced disruption of host translation,[9-11] mitochondrial respiration,[12-14] and the proteasome,[15,16] as well as cell damage[17] and physical distention of the intestinal lumen,[18-20] activate innate immune defenses.

In *C. elegans,* the p38 mitogen-activated protein kinase (MAPK) pathway controls the transcription of secreted immune effectors and is necessary for resistance against multiple pathogens, including *P. aeruginosa.*[21-24] Activation of the p38 PMK-1 pathway in *C. elegans* is controlled by TIR-1 (Toll/IL-1 receptor domain protein), the homolog of mammalian sterile alpha and TIR motif-containing 1 (SARM1).[25-27] We previously showed that TIR-1/SARM1, a multimeric enzyme with intrinsic nicotinamide adenine dinucleotide (NAD^+) hydrolase activity, multimerizes into protein assemblies (puncta) in intestinal epithelia.[28] Functionally, concentration of TIR-1/SARM1 in this manner superactivates its intrinsic NAD+ hydrolase activity, which drives p38 PMK-1 activation and resistance to pathogen infection.[28] In plants, multimerization of TIR domain-containing immune receptors is essential for host defense against pathogen infection.[29,30] In human neurons, SARM1 aggregation promotes axonal degeneration following neuronal injury.[31,32] However, it is not known what initiates TIR-1/SARM1 multimerization to activate immunity in animals.

Lysosome-related organelles are terminal endocytic vesicles that function as sites for storage and secretion of a diverse array of substances in all metazoan animals.[33] In humans, specialized lysosome-related organelles within leukocytes, for example, store toxic effector molecules.[34] In *C. elegans,* lysosome-related organelles, also called gut granules, are acidic compartments that store zinc and heme,[35-38] are involved in ascaroside biosynthesis,[39] and have been implicated in stress resistance. Loss of lysosome-related organelles inhibited transcriptional activation of some putative immune genes.[40] Whether lysosome-related

organelles are involved in pathogen sensing or the activation of innate immune pathways, however, is not known.

Here, we discovered that TIR-1/SARM1 puncta localized to the membranes of lysosome-related organelles in *C. elegans* intestinal epithelial cells. Alkalinization and collapse of lysosome-related organelles induced by pyocyanin, a toxic phenazine metabolite produced exclusively by *Pseudomonas* species,[41] initiates p38 PMK-1 immune pathway activation during pathogen infection by triggering TIR-1/SARM aggregation. These data characterize the mechanism of TIR-1/SARM1 activation of animal immunity and demonstrate that lysosome-related organelles are dynamic scaffolds for TIR-1/SARM1 that enable intestinal epithelial cells to survey for the effects of a bacterial pathogen to activate innate immune defenses.

RESULTS

TIR-1/SARM1 is expressed on lysosome-related organelles in *C. elegans* intestinal epithelial cells.

Previously, we used clustered regularly interspaced short palindromic repeats (CRISPR)-Cas9 to engineer a *C. elegans* strain that expresses TIR-1/SARM1 protein tagged with the fluorophore wrmScarlet at its endogenous genomic locus.[28] We observed that pathogen infection induces TIR-1::wrmScarlet multimerization into large protein assemblies, or puncta, in the intestinal epithelium.[28] Here, we sought to characterize the mechanism by which infection induced TIR-1/SARM1 assembly to activate the p38 PMK-1 innate immune pathway. Detailed characterization of the sub-cellular localization of TIR-1/SARM1 was challenging because of the dim fluorescence of endogenous TIR-1::wrmScarlet and autofluorescence in wild-type *C. elegans* intestinal epithelial cells. We therefore performed immunostaining of TIR-1/SARM1. For these studies, a *C. elegans* strain that we previously generated using CRISPR-Cas9, which contains TIR-1/SARM1 tagged at its endogenous locus with a 3xFLAG sequence,[28] was probed with an anti-FLAG antibody in fixed samples. Immunostaining of TIR-1/SARM1 confirmed that this protein formed puncta in intestinal epithelial cells (**Figure 1A**). Interestingly, we also observed that TIR-1/SARM1 puncta formed multiple vesicular structures in the intestine (**Figure 1A**, dashed arrows), which were not visualized either in animals treated with RNA interference (RNAi) specific for *tir-1* (**Figure 1B**) or in untagged animals (**Figure S1A**).

By immunostaining, we found that the vesicles that expressed TIR-1/SARM1 were lysosome-related organelles. Specifically, we co-immunostained *C. elegans* TIR-1::3xFLAG animals with an anti-FLAG antibody and a previously generated anti-PGP-2 antibody (**Figure 1C and Supplemental Video 1**).[36] PGP-2 is an ATP-binding cassette transporter that is specifically expressed on the membranes of lysosome-related organelles.[36] Three-dimensional reconstruction of z-stacked images from co-immunostained animals revealed that TIR-1/SARM1

localized to the surface of lysosome-related organelles (**Figure 1C and Supplemental Video 1**). We used the machine-learning software Aivia (Leica) to quantify the co-localization between TIR-1/SARM1+ and PGP-2+ vesicles in three dimensions (see Materials and Methods). Of all PGP-2+ vesicles (green in **Figure 1C**), TIR-1/SARM1 (magenta in **Figure 1C**) co-localized with a median of 70.8% of the vesicles (**Figure 1D**). As a control, we used Aivia to quantify the co-localization of PGP-2+ vesicles and non-specific Alexa Fluor 555+ signal in animals that were incubated with both anti-mouse and anti-rabbit secondary antibodies, but stained only with the anti-PGP-2 antibody. We observed a significant difference in the co-localization of green and magenta signals between this control and the treatment conditions, as quantified by Aivia (**Figure 1D**). Finally, we confirmed the validity of the anti-PGP-2 antibody in detecting lysosome-related organelles within intestinal epithelial cells by performing immunostaining on a *C. elegans* strain that carries a translational reporter for PGP-2 (PGP-2::GFP), which demonstrated that PGP-2::GFP co-localized with staining by the anti-PGP-2 antibody (**Figure S1B**). We also confirmed that the *pgp-2* loss-of-function mutants had abrogated staining by the anti-PGP-2 antibody (**Figure S1C**). In summary, our data demonstrate that TIR-1/SARM1 is expressed on lysosome-related organelles in the *C. elegans* intestine.

TIR-1/SARM1 co-localization with lysosome-related organelles can be visualized in live *C. elegans*.

We previously observed that TIR-1/SARM1 activity increases with molecular crowding.[28] Thus, we hypothesized that TIR-1/SARM1 protein levels influenced TIR-1/SARM1-dependent innate immune activation. We therefore investigated mechanisms of TIR-1/SARM1 regulation and made a surprising observation that RNAi-mediated knockdown of *vhp-1*, the phosphatase that dephosphorylates p38 PMK-1,[42] caused robust induction of TIR-1::3xFLAG protein (**Figures 2A and 2B**). This result was unexpected because TIR-1/SARM1 acts upstream of p38

PMK-1 and is required for its activation.[26] We further explored this observation by examining TIR-1::3xFLAG under non-denaturing, or native, conditions. RNAi of *vhp-1* increased TIR-1/SARM1 protein expression and induced the formation of higher-order multimers (**Figure 2C**). Consistent with these data, *vhp-1(RNAi)* increased TIR-1::wrmScarlet protein expression (**Figure 2D**) and significantly induced the formation of TIR-1::wrmScarlet intestinal puncta (**Figures 2D and 2E**). Together, these data suggested that p38 PMK-1 potentiates innate immune activation by increasing TIR-1/SARM1 expression. To test this hypothesis, we crossed the p38/*pmk-1(km25)* null mutant into TIR-1::3xFLAG. The p38/*pmk-1(km25)* mutation suppressed induction of TIR-1::3xFLAG protein by *vhp-1(RNAi)* (**Figures 2A and 2B**). The phosphatase *vhp-1* also dephosphorylates the MAP kinase *kgb-1.*[43] However, the *kgb-1(km21)* null allele did not suppress the induction of TIR-1::3xFLAG protein by *vhp-1(RNAi),* demonstrating that the p38 PMK-1 pathway specifically induces TIR-1/SARM1 in a feedforward cycle (**Figures S2A and S2B**). We also observed that knockdown of *vhp-1* drove *tir-1* transcription in a p38 PMK-1-dependent manner (**Figure 2F**). Thus, activation of *tir-1* transcription by the p38 PMK-1 pathway potentiates innate immune signaling by inducing TIR-1/SARM1 multimerization.

The robust increase in TIR-1::wrmScarlet expression by *vhp-1(RNAi)* enabled co-localization experiments with GFP-labeled cellular compartments, thereby presenting a convenient means to confirm the co-immunostaining experiments, which found that TIR-1/SARM1 was expressed on PGP-2+ lysosome-related organelles (**Figure 1**). We crossed *C. elegans* TIR-1::wrmScarlet with strains that express GFP translational fusion proteins – PGP-2 (PGP-2::GFP), which marks lysosome-related organelles, and LMP-1 (LMP-1::GFP), which marks lysosomes. Treatment of wild-type animals with *vhp-1(RNAi)* revealed that TIR-1::wrmScarlet formed puncta on the membranes of vesicles that expressed PGP-2::GFP (**Figure 3A,** see filled arrows in higher magnification image), but not LMP-1::GFP (**Figure S3**).

Analysis using ImageJ and the JACoP plug-in demonstrated that TIR-1::wrmScarlet significantly co-localized with PGP-2::GFP ($p<0.05$, Pearson correlation coefficient) (**Figure 3B**), but not LMP-1::GFP (p=not significant, Pearson correlation coefficient) (**Figure 3C**). RNAi-mediated knockdown of *tir-1* suppressed TIR-1::wrmScarlet puncta formation (**Figures 3A and 3B**).

In summary, these data confirmed that TIR-1/SARM1 is expressed on lysosome-related organelles.

A hydrophobic domain in TIR-1/SARM1 is required for its localization on the membranes of lysosome-related organelles and p38 PMK-1 activation.

To uncover TIR-1/SARM1 domains/regions that facilitate its association with the lysosome-related organelles, we employed two orthogonal *in silico* methods (DAS[44] and Phobius[45]). Each of these tools identified a hydrophobic domain within the Armadillo motif (ARM) in four of the eight *C. elegans* TIR-1/SARM1 isoforms (isoform a, c, f, and g) (amino acids 374 to 391 in isoform a) (**Figures 4A, S4A, and S4B**). Using CRISPR-Cas9, we deleted the hydrophobic domain (TIR-1$^{\Delta HD}$) in the TIR-1::3xFLAG background. Co-immunostaining of anti-FLAG and anti-PGP-2 in TIR-1$^{\Delta HD}$::3xFLAG animals revealed that deleting the hydrophobic domain reduced the expression of TIR-1/SARM1 on the surface of lysosome-related organelles (**Figures 4B and 4C**). Unbiased quantification of wild-type and TIR-1$^{\Delta HD}$ mutants by the machine-learning software Aivia (Leica) revealed a significant difference in the co-localization of PGP-2 and TIR-1 between these genotypes (**Figure 4C**). These data demonstrate that the TIR-1/SARM1 hydrophobic domain plays a key role in engaging lysosome-related organelles.

We also assessed whether the TIR-1/SARM1 hydrophobic domain is important for p38 PMK-1 activation. *C. elegans* TIR-1$^{\Delta HD}$ mutants had significantly reduced levels of active p38 PMK-1 at baseline (*e.g.*, in the absence of infection) (**Figures 4D and 4E**). In addition, baseline

expression of the p38 PMK-1-dependent transcriptional immune reporter T24B8.5p::*gfp* was subtly suppressed, most noticeably in the anterior intestine (**Figure 4F**). Accordingly, *tir-1*$^{\Delta HD}$ mutants also expressed significantly lower transcription of the p38 PMK-1-dependent targets *irg-4, irg-5,* and T24B8.5 by qRT-PCR (**Figure 4G).** The *tir-1*$^{\Delta HD}$ mutants were also more susceptible to killing by *P. aeruginosa* than wild-type animals (**Figure 4H**). Intriguingly, the susceptibility of *tir-1*$^{\Delta HD}$ to *P. aeruginosa* was similar to that of *tir-1(RNAi)* animals (**Figure 4H**), despite the relatively small decrease in p38 PMK-1 phosphorylation (**Figure 4D**) and T24B8.5p::*gfp* (**Figure 4E**) expression in *tir-1*$^{\Delta HD}$ mutants. These data suggest that the p38 PMK-1 activation by the hydrophobic domain of TIR-1/SARM1 is critical for resistance against pathogen infection.

We confirmed that TIR-1/SARM1 protein was transcribed in *tir-1*$^{\Delta HD}$ mutants at the same level as wild-type animals (**Figure S4C**). Using an anti-FLAG antibody, we also quantified TIR-1::3xFLAG and TIR-1$^{\Delta HD}$::3xFLAG protein by immunoblot. All isoforms were expressed in TIR-1$^{\Delta HD}$ mutants, albeit at subtly lower levels (**Figures 4I and S4D**). Importantly, knockdown of *vhp-1*, which engaged feedforward transcription of *tir-1* (**Figure 2F**) and resulted in increased TIR-1 protein levels (**Figures 2A-2C**), robustly induced TIR-1$^{\Delta HD}$::3xFLAG protein to similar levels as wild-type TIR-1::3xFLAG protein (**Figure 4I**). In addition, knockdown of *tir-1* further suppressed TIR-1 expression in the TIR-1$^{\Delta HD}$ mutant (**Figure 4I**). In summary, these data demonstrate that a hydrophobic domain is required for TIR-1/SARM1 expression on lysosome-related organelles, p38 PMK-1 activation, and resistance to pathogen infection.

The pathogen-derived virulence effector pyocyanin alkalinizes lysosome-related organelles and induces their collapse in intestinal epithelial cells.

To determine how pathogen infection affects lysosome-related organelles in *C. elegans*, we used LysoTracker Red, a dye that marks acidic organelles (including lysosome-related

organelles),[35,46] to stain animals that were infected with strains of *P. aeruginosa* with differing virulence potentials (**Figure 5A**). We observed that the intensity of LysoTracker Red staining was reduced in animals infected with virulent strains of *P. aeruginosa,* but not in the less virulent *P. aeruginosa* PAK (**Figures 5A and 5B**). Of note, *P. aeruginosa*-mediated depletion of LysoTracker Red was not dependent on *pmk-1* or *tir-1* (**Figure S5A**). These data indicate that depletion of lysosome-related organelles during pathogen infection does not occur downstream of p38 PMK-1 (*i.e.*, as a consequence of immune activation), but rather may be an initiating event of innate immune sensing and p38 PMK-1 activation.

In conjunction, we assessed *C. elegans* lysosome-related organelles using the PGP-2::GFP translational reporter (**Figures 5A and 5C**). The volume of PGP-2::GFP+ vesicles was significantly reduced during pathogen infection in a manner dependent on the virulence potential of the bacterial pathogen (**Figure 5C**). As previously reported,[35,46] we also observed that LysoTracker Red+ vesicles co-localized with PGP-2::GFP (**Figure 5A**). Similar to the observations with LysoTracker Red (**Figure S5A**), the reduction in size of PGP-2::GFP+ vesicles during pathogen infection was not dependent on *pmk-1* or *tir-1* (**Figure S5B**)**.** In summary, *P. aeruginosa* infection alkalinizes (**Figures 5A and 5B**) and collapses (**Figures 5A and 5C**) lysosome-related organelles.

To determine if *P. aeruginosa* specifically targets lysosome-related organelles in *C. elegans* during infection, we assessed mutants with deletions in master regulators of virulence. LysoTracker Red staining of lysosome-related organelles was still markedly reduced in *P. aeruginosa ΔgacA* mutants, but not upon exposure to *P. aeruginosa ΔrhlR* mutants (**Figure 5D**). These data suggest that *rhlR* regulates a gene program in *P. aeruginosa* that depletes host lysosome-related organelles. Thus, we screened transposon mutants for 155 *rhlR*-dependent genes to identify individual pseudomonal virulence effectors that target lysosome-related organelle integrity.[47] Four of the 155 mutants screened phenocopied the *ΔrhlR* mutant with

respect to LysoTracker Red staining of *C. elegans* lysosome-related organelles, two of which were mutations in *phzA2* and *phzB2* (**Table S3**). Intriguingly, each of these genes is involved in the production of phenazines, toxic metabolites that are secreted by *P. aeruginosa*. Accordingly, a *P. aeruginosa* strain with a clean deletion in the phenazine biosynthetic operon (*Δphz*) was unable to reduce the size and number of lysosome-related organelles during infection (**Figure 5D**).

To determine if a single phenazine metabolite caused the effects of *P. aeruginosa* on lysosome-related organelles, we treated animals with phenazine-1-carboxylic acid (PCA), phenazine-1-carboxamide (PCN), 1-hydroxyphenazine (1-HP), and pyocyanin (**Figure 5E**). Of the four phenazine metabolites, treatment with only pyocyanin fully recapitulated the pattern of LysoTracker Red staining observed during infection with wild-type *P. aeruginosa* (**Figure 5E**). In addition, treatment with only pyocyanin, and not the other phenazines, restored the suppression of PGP-2+, LysoTracker Red+ lysosome-related organelles in *C. elegans* exposed to the *P. aeruginosa Δphz* mutant (**Figure 5F**). These data suggested that the secreted virulence effector pyocyanin disrupts the pH of lysosome-related organelles in the *C. elegans* intestine. To confirm this observation, we co-stained pyocyanin-treated and control animals with both LysoTracker Red and LysoSensor Green, a dye with a pKa of ~5.2, which is more sensitive to changes in pH. Animals treated with pyocyanin had significantly less staining of both LysoTracker Red and LysoSensor Green (**Figures 5G and 5H**). Importantly, pyocyanin did not change the pH of the media on which animals were grown (**Figure S5C**). These data demonstrated that pyocyanin alkalinizes lysosome-related organelles.

We then used two orthogonal approaches to determine if pyocyanin treatment recapitulated the change in lysosome-related organelle size we observed upon *P. aeruginosa* infection. Treatment with pyocyanin significantly reduced the volume of PGP-2::GFP+ vesicles (**Figures 5I and 5J**). In addition, immunostaining of lysosome-related organelles with an anti-

PGP-2 antibody also revealed that pyocyanin treatment led to the collapse of lysosome-related organelles (**Figures 5K and 5L**). In summary, the pathogen-derived virulence effector pyocyanin alkalinizes and induces the collapse of lysosome-related organelles in *C. elegans* intestinal epithelial cells.

Pyocyanin triggers aggregation of TIR-1/SARM1 on lysosome-related organelles to activate p38 PMK-1 intestinal immunity.

We previously found that TIR-1/SARM1 multimerizes in response to physical crowding, which activates its intrinsic NAD^+ hydrolase activity.[28] In addition, we observed that TIR-1/SARM1 multimerization is augmented with increasing pH.[28] We therefore hypothesized that the pyocyanin-induced collapse and alkalinization of lysosome-related organelles triggers aggregation of TIR-1/SARM1, which activates the p38 PMK-1 immune pathway. Supporting this model of immune activation in *C. elegans*, treatment with pyocyanin, but not the other phenazines, activated p38 PMK-1 phosphorylation in wild-type animals (**Figures 6A and 6B**). In addition, only pyocyanin robustly induced TIR-1::3xFLAG protein in wild-type animals (**Figures 6C and 6D**), consistent with our data demonstrating that p38 PMK-1 phosphorylation drives induction of TIR-1/SARM1 protein (**Figure 2**).

We previously discovered that the phenazine PCN is sensed by the *C. elegans* nuclear hormone receptor NHR-86, a ligand-gated transcription factor.[8] When activated, NHR-86 directly induces an anti-pathogen transcriptional program and provides protection against killing by *P. aeruginosa* independent of p38 PMK-1 immune pathway.[8,48] Consistent with these data, PCN did not increase p38 PMK-1 phosphorylation (**Figures 6A and 6B**) or TIR-1::3xFLAG protein (**Figures 6C and 6D**).

Importantly, the hydrophobic domain of TIR-1/SARM1, which is required for its localization to lysosome-related organelles (**Figure 4**), was also necessary for the activation of p38 PMK-1 by pyocyanin (**Figures 6A and 6B**). In addition, the *tir-1*$^{\Delta HD}$ mutation abrogated the pyocyanin-induced increase in TIR-1 translation and induction of p38 PMK-1 innate immune pathway observed in wild-type animals (**Figures 6C and 6D**).

Importantly, activation of p38 PMK-1 by pyocyanin treatment requires the presence of PGP-2+ lysosome-related organelles. Ablation of this cellular compartment in *pgp-2(kx48)* loss-of-function mutants suppressed the pyocyanin-mediated activation of p38 PMK-1 (**Figures 6E and 6F**). *C. elegans pgp-2(kx48)* mutants also had significantly higher transcription of *tir-1* mRNA compared to wild-type animals (**Figure S4C**), suggesting that a compensatory response is engaged in this genetic background to increase *tir-1* transcription. Together, these data demonstrate that alkalinization and contraction of lysosome-related organelles by the pathogen-derived toxic metabolite pyocyanin is an upstream event that activates p38 PMK-1 innate immune signaling.

We assessed the contribution of lysosome-related organelles toward resistance to pyocyanin. Exposure to pyocyanin at an elevated pH led to rapid killing of wild-type *C. elegans* (**Figure 5M**), consistent with previous studies.[49] Importantly, both *C. elegans pgp-2(kx48)* and *tir-1*$^{\Delta HD}$ mutants were hypersusceptible to pyocyanin-mediated toxicity in this pathogenesis assay, which is also called the “fast kill” assay (**Figure 5M**). *C. elegans pgp-2(kx48)* mutants were also hypersusceptible to killing by *C. elegans* in an intestinal infection assay (the “slow-kill” assay) (**Figure S5D**). Thus, these results indicate that intact lysosome-related organelles, as well as TIR-1/SARM1 co-localization on these vesicles, are important for resistance against the pathogen-derived virulence effector pyocyanin.

We considered a model where pyocyanin treatment liberates TIR-1/SARM1 from lysosome-related organelles to form cytoplasmic puncta and activate the p38 PMK-1 pathway.

We co-immunostained PGP-2 and TIR-1/SARM1 in animals treated with pyocyanin or solvent control. Pyocyanin treatment did not significantly change TIR-1/SARM1 localization to the membranes of lysosome-related organelles (**Figure 6G**), suggesting that TIR-1/SARM1 is not released from the vesicles under these conditions. We then asked whether pyocyanin treatment led to increased TIR-1/SARM1 puncta formation on lysosome-related organelles. Using Aivia (Leica), we quantified the size (volume) of TIR-1/SARM1 puncta on lysosome-related organelles. Treatment with pyocyanin led to a significant increase in TIR-1/SARM1 puncta size on lysosome-related organelles compared to solvent control alone (**Figures 6H and 6I**).

In summary, pyocyanin is a virulence effector produced by *P. aeruginosa* that triggers alkalinization and contraction of lysosome-related organelles, aggregation of TIR-1/SARM1 on these organelles, and activation of p38 PMK-1 intestinal immunity (**Figure 7**).

DISCUSSION

Pathogen sensing is a challenge for barrier tissues, such as the intestinal epithelium, which constantly interface with both commensal organisms and virulent pathogens. Although intestinal epithelial cells encode pattern recognition receptors, the surveillance of microbial patterns alone is insufficient to differentiate virulent from commensal microorganisms because the ligands for these receptors (MAMPs/PAMPs) are not exclusively expressed on pathogens. One strategy, first revealed in studies of plant immunity, is to monitor for the effects of pathogen infection on the host to trigger anti-pathogen defenses.[1] However, it is not known how such mechanisms link sensing of bacterial infection to the activation of protective immune signaling cascades in the intestinal epithelium. Here, we characterized a mechanism of effector-triggered immunity that allows intestinal epithelial cells to identify pathogenic bacteria. We showed that the conserved immune regulator TIR-1/SARM1 is expressed on the membranes of lysosome-related organelles. Upon infection, pyocyanin, a toxic phenazine produced by *P. aeruginosa*, alkalinizes and collapses lysosome-related organelles, which causes TIR-1/SARM1 to form higher-order multimers on the membranes of these organelles. We previously demonstrated that TIR-1/SARM1 multimerization enhances its intrinsic NAD^+ hydrolase activity resulting in activation of the p38 PMK-1 immune pathway.[28] Accordingly, pyocyanin treatment activates p38 PMK-1 signaling in a manner that requires TIR-1/SARM1 expression on lysosome-related organelles. These data characterize an evolutionarily ancient strategy of immune surveillance that allows nematodes to identify a bacterial pathogen from among its bacterial diet.

Our results have important implications for understanding immune regulation in the animal intestine. First, they uncover a prominent role for lysosome-related organelles in pathogen sensing and immune activation, providing a key insight into the biological function of this prominent, yet incompletely understood, subcellular compartment that is present in all metazoans. Previously recognized as sites for storage and secretion of a diverse array of

substances,[33,37-39,50,51] we demonstrated here that lysosome-related organelles are scaffolds for innate immune signaling regulators that change dynamically during infection to enable sensing of pathogen-derived toxins. These data suggest that the evolutionarily ancient function of lysosome-related organelles may be in stress sensing, offering a clue to their function in higher order hosts. Second, our findings characterize the mechanism of immune activation by TIR-1/SARM1 in the animal intestine. TIR-containing immune receptors are essential for plant immunity[52] and SARM1 in human neurons promotes Wallerian degeneration of axon fragments.[53,54] However, the mechanism by which this strongly conserved protein responds to pathogen infection to activate intestinal immunity in animals was not previously known. Finally, our findings define an initiating event of p38 PMK-1 signaling during pathogen infection, solving a 20-year-old mystery of how this core innate immune pathway is activated in *C. elegans,* and reveal an evolutionarily ancient mechanism of effector-triggered immunity that may be among the most primordial forms of immune sensing in animals.

Importantly, we observed two seemingly distinct populations of TIR-1/SARM1 puncta: those associated with lysosome-related organelles and those in the cytoplasm. The TIR-1/SARM1 puncta on the membrane of lysosome-related organelles dramatically increased in size following exposure to pyocyanin. We hypothesize that these cytoplasmic TIR-1/SARM1 puncta are membrane-free, higher ordered protein assembles formed as a consequence of the feedforward propagation of *tir-1* transcription by the p38 PMK-1 immune pathway. Our findings therefore reveal the importance of pathogen-effector triggered multimerization of TIR-1/SARM1 on immune pathway activation in metazoans.

Phenazines are toxic metabolites made exclusively by *Pseudomonas* species.[41] These molecules are produced only when a community of pseudomonal bacteria has grown to a specific density, under the control of so-called quorum sensing mechanisms, and play particularly important roles in bacterial physiology.[55,56] For example, phenazines promote

aerobic respiration within the relatively anoxic interior of a pseudomonal biofilm by serving as electron shuttles.[57] During infection, these molecules are *bona fide* virulence effectors that perturb mitochondrial function.[14,58] We previously found that one phenazine, PCN, is sensed directly in *C. elegans* as a readout of *P. aeruginosa* virulence potential.[8] Here we demonstrate that *C. elegans* sense the toxic effects of another phenazine, pyocyanin, by surveilling the state of lysosome-related organelles to initiate protective innate immune defenses in *C. elegans*. These findings collectively underscore the importance of phenazines to pseudomonal virulence and demonstrate that *C. elegans* evolved specific mechanisms to detect these metabolites, which are essential for bacterial pathogenesis.

In conclusion, our results establish the mechanism by which the effects of a toxin produced by *P. aeruginosa* are detected by *C. elegans* to activate innate immunity. We propose that lysosome-related organelles are primordial immune organelles, uniquely positioned within intestinal epithelia to recognize and respond to the effects of a virulent pathogen on the host.

ACKNOWLEDGEMENTS

The authors thank Greg Hermann for the anti-PGP-2 antibody, Alexander Soukas for *C. elegans* strains and helpful discussions, Kit-Yi Yam for invaluable input in image analyses, and Melanie Trombly and Milka Kostic for critical reading of the manuscript. The research was supported by R01 AI130289 (to R.P.W.), R01 AI159159 (to R.P.W.), R21 AI163430 (to R.P.W.), F30 DK127690 (to S.Y.T.), T32 AI095213 (to S.Y.T.), F30 AI150127 (to N.D.P.), T32 AI132152 (to N.D.P.), and T32 GM107000 (to S.Y.T. and N.D.P.). Some strains were provided by the *Caenorhabditis* Genetics Center, which is funded by the NIH Office of Research Infrastructure Programs (P40 OD010440). The funders had no role in study design, data collection and analysis, decision to publish, or preparation of the manuscript.

AUTHOR CONTRIBUTIONS

Conceptualization: SYT, RPW; Methodology: SYT, RPW; Investigation: SYT, KAW, AP; Visualization: SYT; Funding acquisition: RPW; Project administration: RPW; Supervision: RPW; Writing – original draft, SYT, RPW; Writing – review & editing, SYT, RPW

DECLARATION OF INTERESTS

The authors declare no competing interests.

INCLUSION AND DIVERSITY STATEMENT

We support inclusive, diverse, and equitable conduct of research.

FIGURE LEGENDS

Figure 1. TIR-1/SARM1 is expressed on lysosome-related organelles in *C. elegans* intestinal epithelial cells. (A) Representative images of three fixed *C. elegans* TIR-1::3xFLAG animals immunostained with an anti-FLAG antibody (for TIR-1) and DAPI. Insets in the left panel represent corresponding DIC images. Dotted boxes indicate higher magnifications. Dashed arrows in the middle panel indicate multiple vesicular structures. Dotted circles in the right panel highlight lumen of vesicular structures. **(B)** Vector- and *tir-1(RNAi)*-treated *C. elegans* TIR-1::3xFLAG animals were immunostained with an anti-FLAG antibody (for TIR-1) and DAPI. **(C)** Representative images of three *C. elegans* TIR-1::3xFLAG animals co-immunostained with antibodies against FLAG (for TIR-1) or PGP-2 (for lysosome-related organelles). Images are three-dimensional reconstructions of Z-stacks. The last column shows TIR-1 (magenta) co-localized with PGP-2+ lysosome-related organelles (green). **(D)** Quantification of TIR-1 co-localization on PGP-2+ lysosome-related organelles (LRO) in animals stained only with anti-PGP-2 (control) or co-immunostained with both anti-FLAG and anti-PGP-2 by Aivia (Leica). Scale bars as indicated. Source data for this figure is in Table S2. See also Fig. S1. *equals $p<0.05$ (unpaired t-test).

Figure 2. p38 PMK-1 activation increases TIR-1/SARM1 expression and promotes TIR-1/SARM1 multimerization. (A) Representative immunoblot using an anti-FLAG antibody on whole cell lysates of wild-type and *pmk-1(km25)* mutants in the TIR-1::3xFLAG background treated with vector control or *vhp-1(RNAi)*. **(B)** Densitometric quantification of (A). Error bars represent SEM (n=3). *equals $p<0.05$ (two-way ANOVA with Šídák's multiple comparisons test). **(C)** Blue NativePage immunoblot on *C. elegans* TIR-1::3xFLAG animals treated with vector control, *tir-1(RNAi), vhp-1(RNAi),* or *vhp-1/tir-1* double RNAi. Immunoblot was probed using the anti-FLAG antibody. Arrow indicates TIR-1 multimer. **(D)** Images of *C. elegans* TIR-1::wrmScarlet animals treated with vector control, *vhp-1(RNAi)* or *tir-1(RNAi)*. Insets represent corresponding DIC images. Dotted boxes indicate higher magnifications. Open arrowheads indicate TIR-1 puncta. **(E)** Quantification of the number of TIR-1::wrmScarlet puncta in (D), as previously described.[28] *equals $p<0.05$ (one-way ANOVA with Tukey's multiple comparisons test). **(F)** qRT-PCR analysis of *tir-1* transcription in wild-type and *pmk-1(km25)* mutant animals treated with vector control or *vhp-1(RNAi).* Error bars represent SD. *equals $p<0.05$ (two-way ANOVA with Tukey's multiple comparisons test). Scale bars as indicated. Source data for this figure is in Table S2. See also Fig. S2.

Figure 3. TIR-1/SARM1 co-localization with lysosome-related organelles can be visualized in live *C. elegans*. (A) Images of *C. elegans* TIR-1::wrmScarlet animals crossed into a PGP-2::GFP translational reporter and treated with either vector control, *vhp-1(RNAi),* or *tir-1(RNAi)*. Scale bars as indicated. Insets in the left panel represent corresponding DIC images of boxed areas. Dotted boxes indicate higher magnifications. Open arrowheads indicate TIR-1::wrmScarlet puncta on the membranes of vesicles expressing PGP-2::GFP and filled arrowheads indicate TIR-1::wrmScarlet puncta that do not co-localize with PGP-2. Asterisks (*) indicate autofluorescence. Quantification of TIR-1 co-localization with **(B)** lysosome-related organelles (PGP-2) and **(C)** lysosomes (LMP-1). (B and C) Pearson correlation was calculated in each image using Fiji and the JACoP plug-in. Before analysis, non-specific autofluorescence (blue) was first subtracted from the red channel. Any remaining fluorescence was then assessed for co-localization with the green channel. Error bars represent SEM. *equals $p<0.05$ (one-way ANOVA with Dunnett's multiple comparisons test). Source data for this figure is in Table S2. See also Fig. S3.

Figure 4. A hydrophobic domain in TIR-1/SARM1 is required for its localization on the membranes of lysosome-related organelles and p38 PMK-1 activation. (A) Schematics of the *C. elegans* TIR-1 isoforms with a predicted hydrophobic domain as determined by the transmembrane topology predictors Phobius[45] and DAS.[44] **(B)** Representative images of *C. elegans* TIR-1::3xFLAG animals co-immunostained with both anti-FLAG and anti-PGP-2 antibodies. Images are three-dimensional reconstructions of Z-stacks. White boxes indicate higher magnifications. The last column shows only TIR-1 (magenta) co-localized with PGP-2+ lysosome-related organelles (green). **(C)** Quantification of TIR-1 co-localization on PGP-2+ lysosome-related organelles in wild-type and TIR-1$^{\Delta HD}$ mutants stained with both anti-FLAG and anti-PGP-2 by Aivia (Leica). *equals p<0.05 (unpaired t-test). **(D)** Representative immunoblot using anti-phospho PMK-1 and anti-total PMK-1 antibodies in wild-type and TIR-1$^{\Delta HD}$ mutants treated with vector control or *tir-1(RNAi).* **(E)** Densitometric quantification of (D) (*n*=3)**.** Error bars represent SEM. *equals p<0.05 (unpaired t-test). **(F)** Images of wild-type and TIR-1$^{\Delta HD}$ mutants in the T24B8.5p::*gfp* transcriptional reporter background treated with either vector control or *tir-1(RNAi).* **(G)** qRT-PCR of indicated genes in wild-type and TIR-1$^{\Delta HD}$ mutants. *equals p<0.05 (two-way ANOVA with Šídák's multiple comparisons test). **(H)** Representative *P. aeruginosa* pathogenesis assay of wild-type and TIR-1$^{\Delta HD}$ mutants treated with vector control or *tir-1(RNAi).* The difference between the wild-type and the other genotypes is significant (p<0.05, log-rank test). n=3. Mean lifespans and statistics for all replicates are in Table S1. **(I)** Immunoblot using the anti-FLAG antibody (for TIR-1) on whole cell lysates from wild-type and TIR-1$^{\Delta HD}$ mutants within the TIR-1::3xFLAG background treated with vector control, *tir-1(RNAi)* or *vhp-1(RNAi).* Source data for this figure is in Table S2. See also Figure S4.

Figure 5. The pathogen-derived virulence effector pyocyanin alkalinizes lysosome-related organelles and induces their collapse in intestinal epithelial cells. (A) *C. elegans* PGP-2::GFP translational reporters were stained with LysoTracker Red (LTR, 1 µM) and transferred to the indicated *P. aeruginosa* strains for 4-6 hrs. **(B)** Quantification of LysoTracker Red intensity in (A) using the LasX analysis software (Leica). *equals p<0.05 (one-way ANOVA with Dunnett's multiple comparisons test). **(C)** Quantification of PGP-2+ vesicle size using the LasX three-dimensional analysis software (Leica). *equals p<0.05 (one-way ANOVA with Dunnett's multiple comparisons test). **(D)** Images of wild-type LysoTracker Red-stained *C. elegans* uninfected or infected with indicated *P. aeruginosa* mutants for 4 hrs. **(E)** Images of uninfected wild-type LysoTracker Red-stained animals supplemented with PCA (200 µM), PCN (200 µM), 1-HP (20 µM) or PYO (200 µM) for 4 hrs. **(F)** Images of *P. aeruginosa Δphz*-infected wild-type PGP-2::GFP animals stained with LysoTracker Red in presence or absence phenazine supplementation (same concentrations as (E)). **(G)** Images of wild-type animals treated with solvent control or PYO (200 µM) and stained with both LysoTracker Red (LTR, 1 µM) and LysoSensor Green (LSG, 1 µM). **(H)** Quantification of fluorescence intensity in (G). *equals p<0.05 (two-way ANOVA with Šídák's multiple comparisons test). **(I-J)** Wild-type *C. elegans* PGP-2::GFP animals treated with solvent or PYO (200 µM) for 4 hrs. (I) Representative images and (J) quantification of PGP-2::GFP volume. *equals p<0.05 (unpaired t-test). **(K-L)** Wild-type *C. elegans* treated with solvent or PYO (200 µM) for 4 hrs and immunostained with the anti-PGP-2 antibody. (K) Representative images and (L) quantification of PGP-2+ vesicle volume. *equals p<0.05 (unpaired t-test). Scale bars as indicated. **(M)** Representative pyocyanin toxicity "fast-kill" assay of wild-type, TIR-1$^{\Delta HD}$, and *pgp-2(kx48)* mutants. The difference between the wild-type and the other genotypes is significant (p<0.05, log-rank test). n=3. Mean lifespans and statistics for all replicates are in Table S1. Source data for this figure is in Table S2. See also Figure S5.

Figure 6. Pyocyanin triggers aggregation of TIR-1/SARM1 on lysosome-related organelles and activates p38 PMK-1 intestinal immunity. (A) Representative immunoblot of whole cell

lysates isolated from wild-type and TIR-1$^{\Delta HD}$ mutants treated with the indicated phenazines for 4-6 hrs and probed with anti-phospho PMK-1, anti-total PMK-1, and anti-α-tubulin antibodies. **(B)** Densitometric quantification of conditions in (A) (*n*=2). *equals p<0.05 (two-way ANOVA with Tukey's multiple comparisons test). **(C)** Representative immunoblot of whole cell lysates isolated from wild-type and TIR-1$^{\Delta HD}$ mutants in the TIR-1::3xFLAG background treated with indicated phenazines for 4-6 hrs and probed with anti-FLAG and anti-α-tubulin antibodies. **(D)** Densitometric quantification of conditions in (C). (*n*=3*).* *equals p<0.05 (two-way ANOVA with Tukey's multiple comparisons test). **(E)** Representative immunoblot of whole cell lysates isolated from wild-type and *pgp-2(kx48)* mutants treated with solvent control or PYO for 2-6 hrs probed with anti-phosphorylated PMK-1, anti-total PMK-1, and anti-α-tubulin. **(F)** Densitometric quantification of conditions in (E) (*n=3).* *equals p<0.05 (two-way ANOVA with Šídák's multiple comparisons test). **(G)** Quantification of the ratio of PGP-2+ vesicles co-localized with TIR-1 from co-immunostained samples in the presence or absence of PYO. ns=not significant. **(H)** Representative images of animals treated with solvent control or PYO (200 µM) co-immunostained with anti-FLAG (for TIR-1) and anti-PGP-2. Last column represents Aivia (Leica) render of TIR-1 and PGP-2 co-localization. (**I**) Quantification of TIR-1 puncta size on PGP-2+ vesicles in co-immunostained animals in the presence or absence of PYO. *equals p<0.05 (unpaired t-test). All phenazines were used at 200 µM except for 1-HP (20 µM). Source data for this figure is in Table S2.

Figure 7. Pathogen effector-triggered aggregation of TIR-1/SARM1 on lysosome-related organelles activates intestinal immunity.

538 **STAR METHODS**

539 **KEY RESOURCES TABLE**

REAGENT or RESOURCE	SOURCE	IDENTIFIER
Antibodies		
Anti-FLAG M2, Mouse, Monoclonal, Unconjugated	Sigma-Aldrich	Cat# F1804; RRID:AB_262044
Anti-alpha-Tubulin, Mouse, Monoclonal, Unconjugated	Sigma-Aldrich	Cat# T5168; RRID:AB_477579
Anti-phospho-p38 MAPK (Thr180/Tyr182), Rabbit	Cell Signaling Technology	Cat # 9211S; RRID:AB_331641
Anti-total-p38 MAPK, Rabbit	[48]	N/A
Goat Anti-Rabbit IgG, HRP-linked	Cell Signaling Technology	Cat# 7074; RRID:AB_2099233
Goat Anti-Mouse IgG – H&L, Polyclonal, HRP Conjugated	Abcam	Cat# ab6789; RRID:AB_955439
Anti-PGP-2, Rabbit, Unconjugated	[36]	
Goat Anti-Mouse IgG (H+L) Highly Cross-Adsorbed Secondary Antibody, Alexa Fluor™ Plus 647	Thermo Fisher	Cat# A21235
Goat Anti-Mouse IgG (H+L) Highly Cross-Adsorbed Secondary Antibody, Alexa Fluor™ Plus 555	Thermo Fisher	Cat# A32727
Goat Anti-Rabbit IgG (H+L) Highly Cross-Adsorbed Secondary Antibody, Alexa Fluor™ Plus 647	Thermo Fisher	Cat# A32733TR
SlowFade™ Gold Antifade Mountant with DAPI	Thermo Fisher	Cat# S36938
Normal goat serum	Jackson ImmunoResearch	Cat# 005-000-121
Bacterial and virus strains		
Escherichia coli OP50	[59]	WB Cat# WBStrain00041969; RRID:WB-STRAIN:WBStrain00041969
E. coli HT115(DE3)	[60]	WB Cat# WBStrain00041080; RRID:WB-STRAIN:WBStrain00041080
Pseudomonas aeruginosa (UCBPP-PA14)	[61]	RRID:WB-STRAIN:WBStrain00041978
P. aeruginosa (PAK)	[62]	N/A
P. aeruginosa (PAO1)	[62]	N/A
P. aeruginosa PA14 Δ*phzA1-G1* Δ*phzA2-G2* (Δ*phz*)	[63]	N/A
P. aeruginosa PA14 Δ*gacA*	[22]	N/A
P. aeruginosa PA14 Δ*rhlR*	[61]	N/A
P. aeruginosa PA14 transposon mutants	[64]	N/A

Chemicals, peptides, and recombinant proteins		
5-Fluoro-2'-deoxyuridine (FUDR)	Sigma-Aldrich	Cat# CAF0503
(-) Tetramisole hydrochloride	Sigma-Aldrich	Cat# L9756-10G
Isopropyl-β-D-thiogalactoside (IPTG)	GoldBio	Cat# I2481C200
Trizol	Thermo Fisher Scientific	Cat# 15596018
Proteinase K	New England BioLabs	Cat# P8107S
Ethylenediaminetetraacetic acid (EDTA), 0.5M, pH 8.0	Thermo Fisher Scientific	Cat# 1860851
HALT Protease Inhibitor Cocktail (100X)	Thermo Fisher Scientific	Cat# 78430
Phenol:chloroform:isoamyl alcohol	Thermo Fisher Scientific	Cat# 15593031
Phenazine-1-carboxylic acid	Ark Pharm	Cat# AK-98673
Phenazine-1-carboxamide	Princeton BioMolecular Research	Cat# PBMR030086
1-hydroxyphenazine	TCI America	Cat# H0289
Pyocyanin	Cayman Chemicals	Cat# 10009594
SpCas9 Nuclease	IDT	Cat# 1081058
Streptomycin sulfate	Thermo Fisher Scientific	Cat# AC612240500
Poly-L-Lysine	Sigma	Cat# P4707
SlowFade Gold Antifade Mountant with DAPI	Invitrogen	Cat# S36938
LysoTracker™ Red DND-99	Invitrogen	Cat# L7528
LysoSensor™ Green DND-189	Invitrogen	Cat# L7535
Critical commercial assays		
iScript gDNA Clear cDNA Synthesis Kit	Bio-Rad	Cat# 172-5034
DC Protein Assay	Bio-Rad	Cat# 5000111
iTaq Universal SYBR Green Supermix	Bio-Rad	Cat# 172-5120
SuperSignal West Pico	Thermo Fisher	Cat# 34580
SuperSignal West Femto	Thermo Fisher	Cat# 34094
NativePAGE™ Running Buffer Kit	Invitrogen	Cat# BN2007
Deposited data		
Experimental models: Organisms/Strains		
C. elegans: Strain: N2 (Bristol)	[59]	WB Cat# WBStrain00000001; RRID:WB-STRAIN:WBStrain00000001
C. elegans: AU78 *agIs219* [T24B8.5p::*gfp*::*unc54*-3'UTR; *ttx-3*p::*gfp*::*unc-54*-3'UTR] *III*	[65]	WB Cat# WBStrain00000262
C. elegans: RPW403 *ums63* [TIR-1::wrmScarlet]	[28]	
C. elegans: RPW386 *ums57* [TIR-1::3xFLAG]; *agIs219*	[28]	
C. elegans: MGH41 *alxIs1* [*vha-6*p::PGP-2::GFP;pRF4]	Soukas lab, unpublished	

C. elegans: RPW512 *pwIs50* [LMP-1::GFP + Cbr-unc-119(+)]; *ums63* [TIR-1::wrmScarlet]	This study	
C. elegans: RT258 *pwIs50* [LMP-1::GFP + Cbr-unc-119(+)]	[66]	
C. elegans: RPW513 *alxIs1* [*vha-6*p::PGP-2::GFP]; *ums63* [TIR-1::wrmScarlet]	This study	
C. elegans: RPW502 *ums76* [TIR-1$^{\Delta HD}$::3xFLAG]; *agIs219* [T24B8.5p::*gfp*::*unc54*-3'UTR; *ttx-3*p::*gfp*::*unc-54*-3'UTR]	This study	
Experimental models: Media		
Bacto-peptone	Thermo Fisher Scientific	Cat# 211677
Fisher agar	Fisher	
M9W		
PBS		
Oligonucleotides		
See Table S4	This study	N/A
Recombinant DNA		
Software and algorithms		
Fiji/ImageJ	[67]	RRID:SCR_002285
OASIS 2	[68]	RRID:SCR_014450
GraphPad Prism 9	https://www.graphpad.com/scientific-software/prism/	RRID:SCR_002798
Zen (2.5)	Zeiss	RRID:SCR_013672
LasX (1.4.5)	Leica	RRID:SCR_013673
Aivia (11.0.1)	Leica	N/A
CHOPCHOP (version 3)	[69]	RRID:SCR_015723
DAS	[44]	N/A
Phobius	[45]	RRID:SCR_015643
Other		
Positively charged slides	Fisher	Cat# 22170341
Leica THUNDER DMi8	Leica	

RESOURCE AVAILABILITY

Lead contact

Further information and requests for resources or reagents should be directed to and will be fulfilled by the lead contact, Read Pukkila-Worley (read.pukkila-worley@umassmed.edu).

Material availability

Strains and reagents generated in this study are available upon request.

Data and code availability

This paper does not report original code.

EXPERIMENTAL MODEL AND SUBJECT DETAILS

C. elegans strains

The previously published *C. elegans* strains used in this study were: N2 Bristol,[59] AU78 *agIs219* [T24B8.5p::*gfp*::*unc54*-3'UTR; *ttx-3*p::*gfp*::*unc-54*-3'UTR] *III,*[65] RPW403 *ums63* [TIR-1::wrmScarlet],[28] RPW386 *ums57* [TIR-1::3xFLAG]; *agIs219* [T24B8.5p::*gfp*::*unc54*-3'UTR; *ttx-3*p::*gfp*::*unc-54*-3'UTR] *III,*[28] MGH41 *alxIs1* [*vha-6*p::PGP-2::GFP;pRF4] (unpublished), RT258 *pwIs50* [LMP-1::GFP + Cbr-unc-119(+)].[66] The strains developed in this study were: RPW512 *pwIs50* [LMP-1::GFP + Cbr-unc-119(+)]; *ums63* [TIR-1::wrmScarlet], RPW513 *alxIs1* [*vha-6*p::PGP-2::GFP]; *ums63* [TIR-1::wrmScarlet], RPW502 *ums76* [TIR-1$^{\Delta HD}$::3xFLAG]; *agIs219* [T24B8.5p::*gfp*::*unc54*-3'UTR; *ttx-3*p::*gfp*::*unc-54*-3'UTR].

C. elegans growth conditions

C. elegans strains were maintained on standard nematode growth medium (NGM) plates [0.25% Bacto-peptone, 0.3% sodium chloride, 1.7% agar (Fisher agar), 5 µg/mL cholesterol, 25 mM potassium phosphate pH 6.0, 1 mM magnesium sulfate, 1 mM calcium chloride] with *E. coli* OP50 as a food source, as described.[59]

Bacterial strains

Bacteria used in this study were *Escherichia coli* (*E. coli*) OP50,[59] *E. coli* HT115(DE3),[60] and *Pseudomonas aeruginosa* strains PA14,[61] PAO1,[62] PAK,[62] PA14 Δ*phzA1-G1* Δ*phzA2-G2* (Δ*phz*),[63] PA14 Δ*gacA,*[22] PA14 Δ*rhlR,*[61] and PA14 transposon mutants.[64]

Bacterial growth conditions

E. coli OP50 were grown in LB broth supplemented with 0.175 mg/mL streptomycin at 37 °C for 16-18 hrs at 250 rpm. *P. aeruginosa* strains were grown in LB broth at 37 °C for 14-15 hrs at 250 rpm.

METHODS

C. elegans immunofluorescence analysis

Immunostaining was performed as previously described with adaptations [70]. All *C. elegans* strains were grown on NGM until the L4 to young adult stage. For Figure 6, animals were grown on NGM until the L4 stage and then transferred to "slow-kill" plates containing either 1% DMSO (solvent control) or 200 µM PYO. 30 µL of 0.2% poly-L-lysine was sandwiched between two clean positively charged slides and then allowed to air dry for 30 min. Five to ten slides were prepared for each condition. About 100-200 animals were transferred onto clean, non-seeded (no *E. coli* OP50) plates for about 15-30 min to allow for the removal of excess bacteria from the cuticle. Two flat metal blocks were then placed at the bottom of a container filled with dry ice and 100% ethanol.

On each poly-L-lysine-coated slide, 25-30 animals were picked into a 5 µL droplet of M9W. A 22 x 22 mm glass coverslip was then carefully placed on top of the animals and immediately flash-frozen on the flat metal blocks. Flash-frozen slides were stored at -80 °C until ready for immunostaining. Without thawing the slides, a razor edge was used to quickly flick off the coverslip. Slides were immersed in Coplin jars containing cold 100% methanol for 15 min at -20 °C followed by 100% acetone for another 15 min at -20 °C. Slides were then air-dried at room temperature.

Animals were rehydrated with 50-100 µL 1X PBS and then blocked for 30 min with 5% normal goat serum in 1X PBS at room temperature. Primary antibodies were prepared in 5% normal goat serum in 1X PBS containing 0.2% Tween-20 (PBST) at the following concentrations: 1:250 mouse anti-FLAG M2 (for TIR-1) and 1:500 rabbit anti-PGP-2. Slides were incubated with primary antibody overnight in a humidified chamber at 4 °C. Slides were washed with PBST and then incubated with secondary antibody (anti-rabbit AF647 or anti-mouse AF555) in 5% normal goat serum in PBST for 1 hr at room temperature. Slides were washed again with PBST followed by 1X PBS. Slides were then mounted with SlowFade Gold containing DAPI (Thermo Fisher) and sealed with clear nail polish.

All immunostained slides were subsequently imaged on the THUNDER Imager (Leica DMi8, inverted microscope) using a Leica 63X objective.

Feeding RNAi

C. elegans were fed *E. coli* HT115 expressing dsRNA targeting the genes of interest, as previously described with modifications.[60,71,72] In brief, HT115 bacteria expressing specific dsRNA were grown on LB agar containing 50 µg/mL ampicillin and 15 µg/mL tetracycline at 37 °C overnight. Colonies were then inoculated in LB broth containing 50 µg/mL ampicillin overnight at 37 °C for 16-18 hrs with shaking at 250 rpm. Overnight cultures were then seeded onto NGM plates containing 5 mM IPTG and 50 µg/mL carbenicillin and incubated for 16-18 hrs. Synchronized L1 animals were then transferred onto NGM plates with the grown bacteria and allowed to mature to the L4 stage.

LysoTracker Red and LysoSensor Green assays

Animals were stained with either LysoTracker Red (Thermo Fisher) or LysoSensor Green (Thermo Fisher) as previously described.[35,46] To stain animals with either LysoTracker Red or LysoSensor Green, 60 mm NGM plates (about 10 mL media) were first seeded with *E. coli* OP50 or HT115 and allowed to dry. Stocks were then diluted 1:10 in M9W (100 µM). 100 µL of each dye was then added on top of the dried bacteria and the dye was allowed to percolate through the plates for 1-2 hrs (final concentration 10 µM). L1 synchronized animals were then dropped on NGM plates containing either 1-2% DMSO, 10 µM LysoTracker Red, or 10 µM LysoTracker Red plus 10 µM LysoSensor Green and allowed to grow in the dark until the L4 stage. About 1-2 hrs before imaging, animals were transferred to NGM plates containing freshly seeded *E. coli* OP50. For infection or phenazine supplementation experiments, L4 animals were transferred to challenge conditions for 4-6 hrs at 25 °C before imaging.

For Figures 5A, 5F, and 5G, animals were imaged on the THUNDER Imager (Leica DMi8, inverted microscope) using a Leica 63X objective. For Figures 5D and 5E, animals were imaged using a Zeiss AXIO Imager Z2 microscope.

Microscopy and image analysis

Immunofluorescence. All immunostained slides were imaged using the THUNDER Imager (Leica DMi8, inverted microscope) with a Leica 63X objective and LasX software (Leica). Z-stacks were taken for each animal. The width of each slice was automatically determined by the software. Each stack was about 20 µm. The LasX 3D analysis software was used to quantify the volume of each PGP-2+ vesicle within each animal for the indicated conditions.

Live imaging of animals. For fluorescence imaging, nematodes were mounted onto 2% agarose pads, paralyzed with 50 mM tetramisole (Sigma), and imaged using a Zeiss AXIO Imager Z2 microscope with a Zeiss Axiocam 506 mono camera and Zen 2.5 (Zeiss) software. For LysoTracker Red and/or LysoSensor Green, or TIR-1::wrmScarlet imaging, animals were

mounted onto 2% agarose pads, paralyzed with 50 mM tetramisole (Sigma), and sealed with coverslips and VALAP. Slides were then inverted and imaged on the THUNDER Imager (Leica DMi8, inverted microscope) with a Leica 63X objective and LasX software (Leica).

TIR-1 puncta quantification. TIR-1 puncta quantification was performed as described previously.[28]

Co-localization of TIR-1 and PGP-2 in live animal samples. Co-localization of TIR-1 and PGP-2 in live animals was determined using Fiji (ImageJ). First, red (TIR-1) and blue (autofluorescence) channels were co-localized with the "Color threshold" function. Green (PGP-2 or LMP-1) and blue (autofluorescence) channels were then co-localized. Any co-localized signal with the blue channel was then subtracted from the images. JACoP was then used to determine the Pearson's coefficient of co-localization between red and green channels.[73]

Co-localization of TIR-1 with PGP-2+ vesicles in immunostained samples. Aivia (Leica) was used to quantify co-localization between TIR-1 and PGP-2+ vesicles in the immunostained samples. Briefly, pixel classifiers were used to determine positive signals for both TIR-1 (Alexa Fluor 555) and PGP-2 (Alexa Fluor 647) channels. Meshes were then made for each channel and the number of relations were determined between TIR-1 and PGP-2. The 3D object analysis recipe for TIR-1 was as follows: Image Smoothing Filter Size: 1; Min Edge Intensity: 50; Fill Holes Size: 0; Object radius: 0-2 µm; Mesh smoothing factor: 0; Min Edge to Center Distance: 0.5 µm. The 3D object analysis recipe for PGP-2 was as follows: Image Smoothing Filter Size: 1; Min Edge Intensity: 70; Fill Holes Size: 0; Object radius: 0-5 µm; Mesh smoothing factor: 0; Min Edge to Center Distance: 0.5 µm. Relations on frame were then quantified and graphed with the PGP-2 channel as the primary mesh.

TIR-1 puncta size on PGP-2+ lysosome-related organelles. For quantification of TIR-1 puncta size on lysosome-related organelles, Aivia (Leica) was used to first render the Z-stacks imaged from co-immunostained animals treated with solvent control or pyocyanin in three dimensions. For lysosome-related organelles that co-localized with TIR-1/SARM1, we quantified the size (volume) of all TIR-1/SARM1 objects associated with that vesicle. Quantifications were completed in 5 animals, where 5 random PGP-2+ vesicles in the anterior intestine per animal were chosen.

C. elegans strain construction

All CRISPR genome editing was performed as previously described.[74] CRISPR-Cas9 editing with single-stranded oligodeoxynucleotide (ssODN) homolog-directed repair was used to introduce the hydrophobic domain deletion into *tir-1.* All CRISPR reagents were purchased from Integrated DNA Technologies. Target guide sequences were selected using the CHOPCHOP web tool. The ssODN repair templates contained indicated deletions with 35 bp flanking homology arms. ssODN sequences are listed in Table S4. The F1 progeny were screened for Rol phenotypes 3 to 4 days after injection and then for indicated edits using PCR and Sanger sequencing. Primer sequences used for genotyping are listed in Table S4.

Immunoblot analyses

Protein lysates were prepared using a Teflon Dounce homogenizer from 5-10,000 *C. elegans* grown to the L4 larval stage on NGM plates seeded with *E. coli* OP50, as previously described [8,28]. LDS Sample Buffer (Thermo Fisher Scientific) was added to a concentration of 1X with 5% β-mercaptoethanol. All samples were incubated at 70 °C for 10 minutes. Total protein from each sample was resolved on NuPage Bis-Tris 4–12% gels (Invitrogen), for detection of phosphorylated and total p38 PMK-1, or NuPage Tris-Acetate 3-8% gels (Invitrogen), for

detection of TIR-1. Protein was then transferred to 0.2 µM nitrocellulose membranes (Bio-Rad) and blocked with 5% milk in 1x TBS + 0.2% Tween-20 for one hour. Blots were then probed with a 1:1000 dilution of mouse monoclonal anti-FLAG M2 (Sigma, #F1804), 1:1000 phospho p38 PMK-1 (Cell Signaling Technology, #9211), 1:1000 total PMK-1,[48] 1:2000 mouse monoclonal anti-alpha-Tubulin (Sigma, #T5168), overnight at 4 °C. Anti-mouse IgG-HRP (Abcam, #ab6789) or anti-rabbit IgG-HRP (Cell Signaling Technology, #7074) secondary antibodies were used at a dilution of 1:10,000 to detect the primary antibodies. Blots were then developed with the addition of SuperSignal™ West Pico or West Femto PLUS Chemiluminescent Substrate (Thermo Fisher Scientific) and visualized using a ChemiDoc MP Imaging System (Bio-Rad). Band intensities were quantified using ImageJ (Fiji).

NativePAGE analysis was performed as previously described. Protein lysates were prepared in 1x NativePAGE buffer (Invitrogen), 1% digitonin, and HALT protease inhibitor (Thermo Fisher). Coomassie G-250 additive was added to samples and loaded onto NativePAGE 3-12% Bis-Tris gels (Invitrogen). Samples were first run in dark blue cathode buffer (inner chamber) until the front ran 1/3 down the gel. The buffer was then switched to the light blue cathode buffer. Protein was then transferred onto 0.2 µm PVDF membranes overnight at 4°C. After transfer, membranes were placed in 8% acetic acid and fixed for 15 minutes at room temperature on a rocker. The blot was then destained with 50% methanol/10% acetic acid until the membrane was white and blocked with 5% milk in 1x TBS + 0.2% Tween-20 for 1 hr at room temperature on a rocker. Blots were then transferred to mouse anti-FLAG M2 (Sigma, #F1804) antibody overnight at 4°C. The following day, blots were washed and transferred to anti-mouse IgG-HRP (Abcam, #ab6789) for 1 hr at room temperature on a rocker. Blots were then developed with the addition of SuperSignal™ West Femto PLUS Chemiluminescent Substrate (Thermo Fisher Scientific) and visualized using a ChemiDoc MP Imaging System (Bio-Rad).

qRT-PCR analyses

RNA was extracted from about 2000 L4 animals and reverse transcribed to cDNA using the iScript cDNA Synthesis Kit (Bio-Rad). cDNA was then analyzed on the CFX384 thermocycler (Bio-Rad) with primers described in Table S4. All values were normalized to the geometric mean of the control genes *act-3* and *snb-1*. Relative expression was then calculated using the Pfaffl method.[75]

***C. elegans* pathogenesis assays**

"Slow-killing" *P. aeruginosa* infection experiments were performed as previously described.[76] In brief, *P. aeruginosa* was grown as described above and 10 µL overnight culture was spread onto the center of 35-mm tissue culture plates containing 4 mL slow-kill agar (0.35% Bacto-peptone, 0.3% sodium chloride, 1.7% agar, 5 µg/mL cholesterol, 25 mM potassium phosphate, 1 mM magnesium sulfate, 1 mM calcium chloride). Plates were then incubated for 24 hrs at 37 °C followed by 24 hrs at 25 °C. Wild-type and *pgp-2(kx48) C. elegans* were then transferred to *P. aeruginosa* slow-kill plates containing FUDR. Dead animals were scored twice daily until completion. Three trials of the assay were performed. Sample sizes, mean survival, and p-values for all trials are shown in Table S1.

"Fast-killing" *P. aeruginosa* infection experiments were performed as previously described.[8,49,76] Briefly, PA14 Δ*phz* mutants were grown on PGS agar (1% Bacto-peptone, 1% glucose, 1% NaCl, 150 mM sorbitol, 1.7% Bacto-agar) for 24 hrs at 37 °C followed by 24 hrs at 25 °C. The lawns were then scraped off of the agar. The remaining agar was then melted, and the pH was adjusted to pH 7.0 using 100 mM potassium phosphate. Either DMSO (solvent) or 50 µM PYO was then added to the agar. Once cooled and solidified, plates were seeded with 10X *E. coli*

OP50. Wild-type, TIR-1$^{\Delta HD}$ mutants or *pgp-2(kx48)* mutants were then transferred to the plates at the L4 stage and scored for survival at room temperature (22 °C).

Quantification, statistical analysis, and visualization

Differences in the survival of *C. elegans* in the *P. aeruginosa* pathogenesis assays were determined with the log-rank test after survival curves were estimated for each group with the Kaplan-Meier method. OASIS 2 was used for these statistical analyses.[68] Statistical hypothesis testing was performed with Prism 9 (GraphPad Software) using methods indicated in the figure legends. Table S2 contains all source data and statistical analysis methods and results. Sample sizes, survival, and p-values for all trials are shown in Table S1. BioRender was used to create the image in Figure 7.

SUPPORTING INFORMATION

Figure S1. TIR-1/SARM1 is expressed on lysosome-related organelles in *C. elegans* intestinal epithelial cells. (A) Three representative images of untagged animals immunostained with anti-FLAG (for TIR-1) antibody. Dotted white boxes indicate higher magnifications. **(B)** Three representative images of PGP-2::GFP animals immunostained with anti-PGP-2 antibody. Insets in left panel represent corresponding DIC images. **(C)** Representative images of wild-type and *pgp-2(kx48)* loss-of-function mutants immunostained with anti-PGP-2 antibody. Dotted white boxes indicate higher magnifications. Insets in left panel represent corresponding DIC images. Scale bars as indicated. Related to Fig. 1.

Figure S2. p38 PMK-1 activation increases TIR-1/SARM1 expression and promotes TIR-1/SARM1 multimerization. (A) Immunoblots of whole cell lysates from wild-type, *pmk-1(km25)*, and *kgb-1(km21)* animals treated with vector control or *vhp-1(RNAi)* and probed for anti-FLAG and anti-β-tubulin. **(B)** Immunoblots of whole cell lysates from wild-type, *pmk-1(km25)*, and *kgb-1(km21)* animals treated with vector control or *vhp-1(RNAi)* and probed for anti-phosphorylated PMK-1, anti-total PMK-1 and anti-β-tubulin. Related to Fig. 2.

Figure S3. TIR-1/SARM1 co-localization with lysosome-related organelles can be visualized in live *C. elegans*. Images of *C. elegans* TIR-1::wrmScarlet animals crossed into a LMP-1::GFP translational reporter and treated with either vector control, *vhp-1(RNAi)* or *tir-1(RNAi)*. Dotted white boxes indicate higher magnifications. Scale bars as indicated. Related to Fig. 3.

Figure S4. A hydrophobic domain in TIR-1/SARM1 is required for its localization on the membranes of lysosome-related organelles and p38 PMK-1 activation. (A) Prediction of hydrophobic domains in TIR-1a by DAS. **(B)** Prediction of hydrophobic domains by Phobius. **(C)** qRT-PCR of *tir-1* in wild-type, TIR-1$^{\Delta HD}$, or *pgp-2(kx48)* mutants. *equals $p<0.05$ (one-way ANOVA with Dunnett's multiple comparisons test). **(D)** Predicted molecular weights of TIR-1 isoforms from WormBase. Related to Fig. 4.

Figure S5. The pathogen-derived virulence effector pyocyanin alkalinizes lysosome-related organelles and induces their collapse in intestinal epithelial cells. (A) Representative images of wild-type, *tir-1(qd4)* and *pmk-1(km25)* animals stained with LysoTracker Red and uninfected or infected with *P. aeruginosa* (PA14). **(B)** Representative images of PGP-2::GFP animals treated with vector control, *tir-1(RNAi)* and *pmk-1(RNAi)* infected with *P. aeruginosa.* **(C)** pH of liquid "slow kill" media supplemented with indicated phenazines. **(D)** Representative *P. aeruginosa* pathogenesis assay on wild-type vs. *pgp-2(kx48)* mutants. The difference between wild-type and *pgp-2(kx48)* is significant ($p<0.05$, log-rank test). n=3. Mean lifespans and statistics for all replicates are in Table S1. Related to Fig. 5.

Table S1. Sample sizes, mean lifespans, and p-value for the *C. elegans* pathogenesis assays.

Table S2. Source data and statistical tests used for each figure and supplemental figure.

Table S3. *P. aeruginosa* transposon mutant hits that rescued LysoTracker Red phenotype.

Table S4. Primer, crRNA guide and ssODN sequences designed for this study.

Video S1. Three-dimensional reconstruction of co-immunostained anti-FLAG (TIR-1) and anti-PGP-2 animal.

References

1. Remick, B.C., Gaidt, M.M., and Vance, R.E. (2023). Effector-Triggered Immunity. Annu Rev Immunol *41*, 453-481. 10.1146/annurev-immunol-101721-031732.
2. Lopes Fischer, N., Naseer, N., Shin, S., and Brodsky, I.E. (2020). Effector-triggered immunity and pathogen sensing in metazoans. Nat Microbiol *5*, 14-26. 10.1038/s41564-019-0623-2.
3. Orzalli, M.H., and Parameswaran, P. (2022). Effector-triggered immunity in mammalian antiviral defense. Trends Immunol *43*, 1006-1017. 10.1016/j.it.2022.10.004.
4. Brennan, J.J., and Gilmore, T.D. (2018). Evolutionary Origins of Toll-like Receptor Signaling. Mol Biol Evol *35*, 1576-1587. 10.1093/molbev/msy050.
5. Irazoqui, J.E., Urbach, J.M., and Ausubel, F.M. (2010). Evolution of host innate defence: insights from *Caenorhabditis elegans* and primitive invertebrates. Nat Rev Immunol *10*, 47-58. nri2689 10.1038/nri2689.
6. Pukkila-Worley, R. (2016). Surveillance Immunity: An Emerging Paradigm of Innate Defense Activation in *Caenorhabditis elegans*. PLoS Pathog *12*, e1005795. 10.1371/journal.ppat.1005795.
7. Pujol, N., Link, E.M., Liu, L.X., Kurz, C.L., Alloing, G., Tan, M.W., Ray, K.P., Solari, R., Johnson, C.D., and Ewbank, J.J. (2001). A reverse genetic analysis of components of the Toll signaling pathway in *Caenorhabditis elegans*. Curr Biol *11*, 809-821.
8. Peterson, N.D., Tse, S.Y., Huang, Q.J., Wani, K.A., Schiffer, C.A., and Pukkila-Worley, R. (2023). Non-canonical pattern recognition of a pathogen-derived metabolite by a nuclear hormone receptor identifies virulent bacteria in *C. elegans*. Immunity. https://doi.org/10.1016/j.immuni.2023.01.027.
9. Estes, K.A., Dunbar, T.L., Powell, J.R., Ausubel, F.M., and Troemel, E.R. (2010). bZIP transcription factor zip-2 mediates an early response to Pseudomonas aeruginosa infection in *Caenorhabditis elegans*. Proc Natl Acad Sci U S A *107*, 2153-2158. 0914643107 10.1073/pnas.0914643107.
10. Dunbar, T.L., Yan, Z., Balla, K.M., Smelkinson, M.G., and Troemel, E.R. (2012). *C. elegans* detects pathogen-induced translational inhibition to activate immune signaling. Cell Host Microbe *11*, 375-386. 10.1016/j.chom.2012.02.008.
11. McEwan, D.L., Kirienko, N.V., and Ausubel, F.M. (2012). Host translational inhibition by *Pseudomonas aeruginosa* Exotoxin A Triggers an immune response in *Caenorhabditis elegans*. Cell Host Microbe *11*, 364-374. 10.1016/j.chom.2012.02.007.
12. Mao, K., Breen, P., and Ruvkun, G. (2022). The *Caenorhabditis elegans* ARIP-4 DNA helicase couples mitochondrial surveillance to immune, detoxification, and antiviral pathways. Proc Natl Acad Sci U S A *119*, e2215966119. 10.1073/pnas.2215966119.
13. Mao, K., Ji, F., Breen, P., Sewell, A., Han, M., Sadreyev, R., and Ruvkun, G. (2019). Mitochondrial Dysfunction in C. elegans Activates Mitochondrial Relocalization and Nuclear Hormone Receptor-Dependent Detoxification Genes. Cell Metab *29*, 1182-1191 e1184. 10.1016/j.cmet.2019.01.022.
14. Deng, P., Uma Naresh, N., Du, Y., Lamech, L.T., Yu, J., Zhu, L.J., Pukkila-Worley, R., and Haynes, C.M. (2019). Mitochondrial UPR repression during *Pseudomonas aeruginosa* infection requires the bZIP protein ZIP-3. Proc Natl Acad Sci U S A *116*, 6146-6151. 10.1073/pnas.1817259116.

15. Melo, J.A., and Ruvkun, G. (2012). Inactivation of conserved *C. elegans* genes engages pathogen- and xenobiotic-associated defenses. Cell *149*, 452-466. 10.1016/j.cell.2012.02.050.
16. Bakowski, M.A., Desjardins, C.A., Smelkinson, M.G., Dunbar, T.L., Lopez-Moyado, I.F., Rifkin, S.A., Cuomo, C.A., and Troemel, E.R. (2014). Ubiquitin-mediated response to microsporidia and virus infection in *C. elegans*. PLoS Pathog *10*, e1004200. 10.1371/journal.ppat.1004200.
17. Zugasti, O., Bose, N., Squiban, B., Belougne, J., Kurz, C.L., Schroeder, F.C., Pujol, N., and Ewbank, J.J. (2014). Activation of a G protein-coupled receptor by its endogenous ligand triggers the innate immune response of *Caenorhabditis elegans*. Nat Immunol *15*, 833-838. 10.1038/ni.2957.
18. Singh, J., and Aballay, A. (2019). Intestinal infection regulates behavior and learning via neuroendocrine signaling. Elife *8*. 10.7554/eLife.50033.
19. Filipowicz, A., Lalsiamthara, J., and Aballay, A. (2021). TRPM channels mediate learned pathogen avoidance following intestinal distention. Elife *10*. 10.7554/eLife.65935.
20. Singh, J., and Aballay, A. (2019). Microbial Colonization Activates an Immune Fight-and-Flight Response via Neuroendocrine Signaling. Dev Cell *49*, 89-99 e84. 10.1016/j.devcel.2019.02.001.
21. Kim, D.H., Feinbaum, R., Alloing, G., Emerson, F.E., Garsin, D.A., Inoue, H., Tanaka-Hino, M., Hisamoto, N., Matsumoto, K., Tan, M.W., and Ausubel, F.M. (2002). A conserved p38 MAP kinase pathway in *Caenorhabditis elegans* innate immunity. Science *297*, 623-626. 10.1126/science.1073759.
22. Troemel, E.R., Chu, S.W., Reinke, V., Lee, S.S., Ausubel, F.M., and Kim, D.H. (2006). p38 MAPK regulates expression of immune response genes and contributes to longevity in *C. elegans*. PLoS Genet *2*, e183. 10.1371/journal.pgen.0020183.
23. Peterson, N.D., and Pukkila-Worley, R. (2018). *Caenorhabditis elegans* in high-throughput screens for anti-infective compounds. Curr Opin Immunol *54*, 59-65. 10.1016/j.coi.2018.06.003.
24. Pukkila-Worley, R., Feinbaum, R., Kirienko, N.V., Larkins-Ford, J., Conery, A.L., and Ausubel, F.M. (2012). Stimulation of host immune defenses by a small molecule protects *C. elegans* from bacterial infection. PLoS Genet *8*, e1002733. 10.1371/journal.pgen.1002733.
25. Mink, M., Fogelgren, B., Olszewski, K., Maroy, P., and Csiszar, K. (2001). A novel human gene (SARM) at chromosome 17q11 encodes a protein with a SAM motif and structural similarity to Armadillo/beta-catenin that is conserved in mouse, *Drosophila*, and *Caenorhabditis elegans*. Genomics *74*, 234-244. 10.1006/geno.2001.6548.
26. Liberati, N.T., Fitzgerald, K.A., Kim, D.H., Feinbaum, R., Golenbock, D.T., and Ausubel, F.M. (2004). Requirement for a conserved Toll/interleukin-1 resistance domain protein in the *Caenorhabditis elegans* immune response. Proc Natl Acad Sci USA *101*, 6593-6598. 10.1073/pnas.0308625101.
27. Couillault, C., Pujol, N., Reboul, J., Sabatier, L., Guichou, J.F., Kohara, Y., and Ewbank, J.J. (2004). TLR-independent control of innate immunity in *Caenorhabditis elegans* by the TIR domain adaptor protein TIR-1, an ortholog of human SARM. Nat. Immunol. *5*, 488-494. 10.1038/ni1060.
28. Peterson, N.D., Icso, J.D., Salisbury, J.E., Rodriguez, T., Thompson, P.R., and Pukkila-Worley, R. (2022). Pathogen infection and cholesterol deficiency activate the *C. elegans*

p38 immune pathway through a TIR-1/SARM1 phase transition. Elife *11*. 10.7554/eLife.74206.

29. Martin, R., Qi, T., Zhang, H., Liu, F., King, M., Toth, C., Nogales, E., and Staskawicz, B.J. (2020). Structure of the activated ROQ1 resistosome directly recognizing the pathogen effector XopQ. Science *370*. 10.1126/science.abd9993.

30. Ma, S., Lapin, D., Liu, L., Sun, Y., Song, W., Zhang, X., Logemann, E., Yu, D., Wang, J., Jirschitzka, J., et al. (2020). Direct pathogen-induced assembly of an NLR immune receptor complex to form a holoenzyme. Science *370*. 10.1126/science.abe3069.

31. Horsefield, S., Burdett, H., Zhang, X., Manik, M.K., Shi, Y., Chen, J., Qi, T., Gilley, J., Lai, J.S., Rank, M.X., et al. (2019). NAD(+) cleavage activity by animal and plant TIR domains in cell death pathways. Science *365*, 793-799. 10.1126/science.aax1911.

32. Sporny, M., Guez-Haddad, J., Lebendiker, M., Ulisse, V., Volf, A., Mim, C., Isupov, M.N., and Opatowsky, Y. (2019). Structural Evidence for an Octameric Ring Arrangement of SARM1. J Mol Biol *431*, 3591-3605. 10.1016/j.jmb.2019.06.030.

33. Marks, M.S., Heijnen, H.F., and Raposo, G. (2013). Lysosome-related organelles: unusual compartments become mainstream. Curr Opin Cell Biol *25*, 495-505. 10.1016/j.ceb.2013.04.008.

34. Watts, C. (2022). Lysosomes and lysosome-related organelles in immune responses. FEBS Open Bio *12*, 678-693. 10.1002/2211-5463.13388.

35. Hermann, G.J., Schroeder, L.K., Hieb, C.A., Kershner, A.M., Rabbitts, B.M., Fonarev, P., Grant, B.D., and Priess, J.R. (2005). Genetic analysis of lysosomal trafficking in Caenorhabditis elegans. Mol Biol Cell *16*, 3273-3288. 10.1091/mbc.e05-01-0060.

36. Schroeder, L.K., Kremer, S., Kramer, M.J., Currie, E., Kwan, E., Watts, J.L., Lawrenson, A.L., and Hermann, G.J. (2007). Function of the *Caenorhabditis elegans* ABC transporter PGP-2 in the biogenesis of a lysosome-related fat storage organelle. Mol Biol Cell *18*, 995-1008. 10.1091/mbc.e06-08-0685.

37. Roh, H.C., Collier, S., Guthrie, J., Robertson, J.D., and Kornfeld, K. (2012). Lysosome-related organelles in intestinal cells are a zinc storage site in *C. elegans*. Cell Metab *15*, 88-99. 10.1016/j.cmet.2011.12.003.

38. Sun, F., Zhao, Z., Willoughby, M.M., Shen, S., Zhou, Y., Shao, Y., Kang, J., Chen, Y., Chen, M., Yuan, X., et al. (2022). HRG-9 homologues regulate haem trafficking from haem-enriched compartments. Nature *610*, 768-774. 10.1038/s41586-022-05347-z.

39. Panda, O., Akagi, A.E., Artyukhin, A.B., Judkins, J.C., Le, H.H., Mahanti, P., Cohen, S.M., Sternberg, P.W., and Schroeder, F.C. (2017). Biosynthesis of Modular Ascarosides in *C. elegans*. Angew Chem Int Ed Engl *56*, 4729-4733. 10.1002/anie.201700103.

40. Hajdú, G., Somogyvári, M., Csermely, P., and Sőti, C. (2023). Lysosome-related organelles promote stress and immune responses in *C. elegans*. Commun Biol *6*, 936. 10.1038/s42003-023-05246-7.

41. Pierson, L.S., 3rd, and Pierson, E.A. (2010). Metabolism and function of phenazines in bacteria: impacts on the behavior of bacteria in the environment and biotechnological processes. Appl Microbiol Biotechnol *86*, 1659-1670. 10.1007/s00253-010-2509-3.

42. Kim, D.H., Liberati, N.T., Mizuno, T., Inoue, H., Hisamoto, N., Matsumoto, K., and Ausubel, F.M. (2004). Integration of *Caenorhabditis elegans* MAPK pathways mediating immunity and stress resistance by MEK-1 MAPK kinase and VHP-1 MAPK phosphatase. Proc Natl Acad Sci USA *101*, 10990-10994. 10.1073/pnas.0403546101.

43. Mizuno, T., Hisamoto, N., Terada, T., Kondo, T., Adachi, M., Nishida, E., Kim, D.H., Ausubel, F.M., and Matsumoto, K. (2004). The *Caenorhabditis elegans* MAPK phosphatase VHP-1 mediates a novel JNK-like signaling pathway in stress response. EMBO J *23*, 2226-2234. 10.1038/sj.emboj.7600226.
44. Cserzö, M., Wallin, E., Simon, I., von Heijne, G., and Elofsson, A. (1997). Prediction of transmembrane alpha-helices in prokaryotic membrane proteins: the dense alignment surface method. Protein Eng *10*, 673-676. 10.1093/protein/10.6.673.
45. Käll, L., Krogh, A., and Sonnhammer, E.L. (2004). A combined transmembrane topology and signal peptide prediction method. J Mol Biol *338*, 1027-1036. 10.1016/j.jmb.2004.03.016.
46. Soukas, A.A., Carr, C.E., and Ruvkun, G. (2013). Genetic regulation of *Caenorhabditis elegans* lysosome related organelle function. PLoS Genet *9*, e1003908. 10.1371/journal.pgen.1003908.
47. Mukherjee, S., Moustafa, D., Smith, C.D., Goldberg, J.B., and Bassler, B.L. (2017). The RhlR quorum-sensing receptor controls *Pseudomonas aeruginosa* pathogenesis and biofilm development independently of its canonical homoserine lactone autoinducer. PLoS Pathog *13*, e1006504. 10.1371/journal.ppat.1006504.
48. Peterson, N.D., Cheesman, H.K., Liu, P., Anderson, S.M., Foster, K.J., Chhaya, R., Perrat, P., Thekkiniath, J., Yang, Q., Haynes, C.M., and Pukkila-Worley, R. (2019). The nuclear hormone receptor NHR-86 controls anti-pathogen responses in *C. elegans.* PLoS Genet *15*, e1007935. 10.1371/journal.pgen.1007935.
49. Cezairliyan, B., Vinayavekhin, N., Grenfell-Lee, D., Yuen, G.J., Saghatelian, A., and Ausubel, F.M. (2013). Identification of *Pseudomonas aeruginosa* phenazines that kill *Caenorhabditis elegans.* PLoS Pathog *9*, e1003101. 10.1371/journal.ppat.1003101.
50. Coburn, C., Allman, E., Mahanti, P., Benedetto, A., Cabreiro, F., Pincus, Z., Matthijssens, F., Araiz, C., Mandel, A., Vlachos, M., et al. (2013). Anthranilate fluorescence marks a calcium-propagated necrotic wave that promotes organismal death in *C. elegans.* PLoS Biol *11*, e1001613. 10.1371/journal.pbio.1001613.
51. Chitwood, B.G., and Chitwood, M.B. (1950). An introduction to nematology. Section I. Anatomy. An introduction to nematology. Section I. Anatomy.
52. Essuman, K., Milbrandt, J., Dangl, J.L., and Nishimura, M.T. (2022). Shared TIR enzymatic functions regulate cell death and immunity across the tree of life. Science *377*, eabo0001. 10.1126/science.abo0001.
53. Loring, H.S., Czech, V.L., Icso, J.D., O'Connor, L., Parelkar, S.S., Byrne, A.B., and Thompson, P.R. (2021). A phase transition enhances the catalytic activity of SARM1, an NAD(+) glycohydrolase involved in neurodegeneration. Elife *10*. 10.7554/eLife.66694.
54. Gerdts, J., Summers, D.W., Sasaki, Y., DiAntonio, A., and Milbrandt, J. (2013). Sarm1-mediated axon degeneration requires both SAM and TIR interactions. J Neurosci *33*, 13569-13580. 10.1523/jneurosci.1197-13.2013.
55. Mavrodi, D.V., Blankenfeldt, W., and Thomashow, L.S. (2006). Phenazine compounds in fluorescent Pseudomonas spp. biosynthesis and regulation. Annu Rev Phytopathol *44*, 417-445. 10.1146/annurev.phyto.44.013106.145710.
56. Recinos, D.A., Sekedat, M.D., Hernandez, A., Cohen, T.S., Sakhtah, H., Prince, A.S., Price-Whelan, A., and Dietrich, L.E. (2012). Redundant phenazine operons in *Pseudomonas aeruginosa* exhibit environment-dependent expression and differential

roles in pathogenicity. Proc Natl Acad Sci U S A *109*, 19420-19425. 10.1073/pnas.1213901109.

57. Saunders, S.H., Tse, E.C.M., Yates, M.D., Otero, F.J., Trammell, S.A., Stemp, E.D.A., Barton, J.K., Tender, L.M., and Newman, D.K. (2020). Extracellular DNA Promotes Efficient Extracellular Electron Transfer by Pyocyanin in *Pseudomonas aeruginosa* Biofilms. Cell *182*, 919-932 e919. 10.1016/j.cell.2020.07.006.

58. Ray, A., Rentas, C., Caldwell, G.A., and Caldwell, K.A. (2015). Phenazine derivatives cause proteotoxicity and stress in *C. elegans.* Neurosci Lett *584*, 23-27. 10.1016/j.neulet.2014.09.055.

59. Brenner, S. (1974). The genetics of *Caenorhabditis elegans.* Genetics *77*, 71-94.

60. Fire, A., Xu, S., Montgomery, M.K., Kostas, S.A., Driver, S.E., and Mello, C.C. (1998). Potent and specific genetic interference by double-stranded RNA in *Caenorhabditis elegans*. Nature *391*, 806-811. 10.1038/35888.

61. Rahme, L.G., Stevens, E.J., Wolfort, S.F., Shao, J., Tompkins, R.G., and Ausubel, F.M. (1995). Common virulence factors for bacterial pathogenicity in plants and animals. Science *268*, 1899-1902.

62. Lee, D.G., Urbach, J.M., Wu, G., Liberati, N.T., Feinbaum, R.L., Miyata, S., Diggins, L.T., He, J., Saucier, M., Deziel, E., et al. (2006). Genomic analysis reveals that *Pseudomonas aeruginosa* virulence is combinatorial. Genome Biol *7*, R90. 10.1186/gb-2006-7-10-r90.

63. Dietrich, L.E., Price-Whelan, A., Petersen, A., Whiteley, M., and Newman, D.K. (2006). The phenazine pyocyanin is a terminal signalling factor in the quorum sensing network of *Pseudomonas aeruginosa*. Mol Microbiol *61*, 1308-1321. 10.1111/j.1365-2958.2006.05306.x.

64. Liberati, N.T., Urbach, J.M., Miyata, S., Lee, D.G., Drenkard, E., Wu, G., Villanueva, J., Wei, T., and Ausubel, F.M. (2006). An ordered, nonredundant library of *Pseudomonas aeruginosa* strain PA14 transposon insertion mutants. Proc Natl Acad Sci U S A *103*, 2833-2838. 10.1073/pnas.0511100103.

65. Shivers, R.P., Kooistra, T., Chu, S.W., Pagano, D.J., and Kim, D.H. (2009). Tissue-specific activities of an immune signaling module regulate physiological responses to pathogenic and nutritional bacteria in *C. elegans*. Cell Host Microbe *6*, 321-330. 10.1016/j.chom.2009.09.001.

66. Treusch, S., Knuth, S., Slaugenhaupt, S.A., Goldin, E., Grant, B.D., and Fares, H. (2004). *Caenorhabditis elegans* functional orthologue of human protein h-mucolipin-1 is required for lysosome biogenesis. Proc Natl Acad Sci U S A *101*, 4483-4488. 10.1073/pnas.0400709101.

67. Schindelin, J., Arganda-Carreras, I., Frise, E., Kaynig, V., Longair, M., Pietzsch, T., Preibisch, S., Rueden, C., Saalfeld, S., Schmid, B., et al. (2012). Fiji: an open-source platform for biological-image analysis. Nat Methods *9*, 676-682. 10.1038/nmeth.2019.

68. Han, S.K., Lee, D., Lee, H., Kim, D., Son, H.G., Yang, J.S., Lee, S.V., and Kim, S. (2016). OASIS 2: online application for survival analysis 2 with features for the analysis of maximal lifespan and healthspan in aging research. Oncotarget *7*, 56147-56152. 10.18632/oncotarget.11269.

69. Labun, K., Montague, T.G., Krause, M., Torres Cleuren, Y.N., Tjeldnes, H., and Valen, E. (2019). CHOPCHOP v3: expanding the CRISPR web toolbox beyond genome editing. Nucleic Acids Res *47*, W171-W174. 10.1093/nar/gkz365.

70. Zhang, N., Khan, L.A., Membreno, E., Jafari, G., Yan, S., Zhang, H., and Gobel, V. (2017). The C. elegans Intestine As a Model for Intercellular Lumen Morphogenesis and In Vivo Polarized Membrane Biogenesis at the Single-cell Level: Labeling by Antibody Staining, RNAi Loss-of-function Analysis and Imaging. J Vis Exp. 10.3791/56100.
71. Timmons, L., Court, D.L., and Fire, A. (2001). Ingestion of bacterially expressed dsRNAs can produce specific and potent genetic interference in *Caenorhabditis elegans*. Gene *263*, 103-112. 10.1016/s0378-1119(00)00579-5.
72. Conte, D., Jr., MacNeil, L.T., Walhout, A.J.M., and Mello, C.C. (2015). RNA Interference in *Caenorhabditis elegans.* Curr Protoc Mol Biol *109*, 26 23 21-26 23 30. 10.1002/0471142727.mb2603s109.
73. Bolte, S., and Cordelières, F.P. (2006). A guided tour into subcellular colocalization analysis in light microscopy. J Microsc *224*, 213-232. 10.1111/j.1365-2818.2006.01706.x.
74. Ghanta, K.S., Ishidate, T., and Mello, C.C. (2021). Microinjection for precision genome editing in *Caenorhabditis elegans*. STAR Protoc *2*, 100748. 10.1016/j.xpro.2021.100748.
75. Pfaffl, M.W. (2001). A new mathematical model for relative quantification in real-time RT-PCR. Nucleic Acids Res *29*, e45.
76. Tan, M.W., Mahajan-Miklos, S., and Ausubel, F.M. (1999). Killing of *Caenorhabditis elegans* by *Pseudomonas aeruginosa* used to model mammalian bacterial pathogenesis. Proc Natl Acad Sci USA *96*, 715-720.

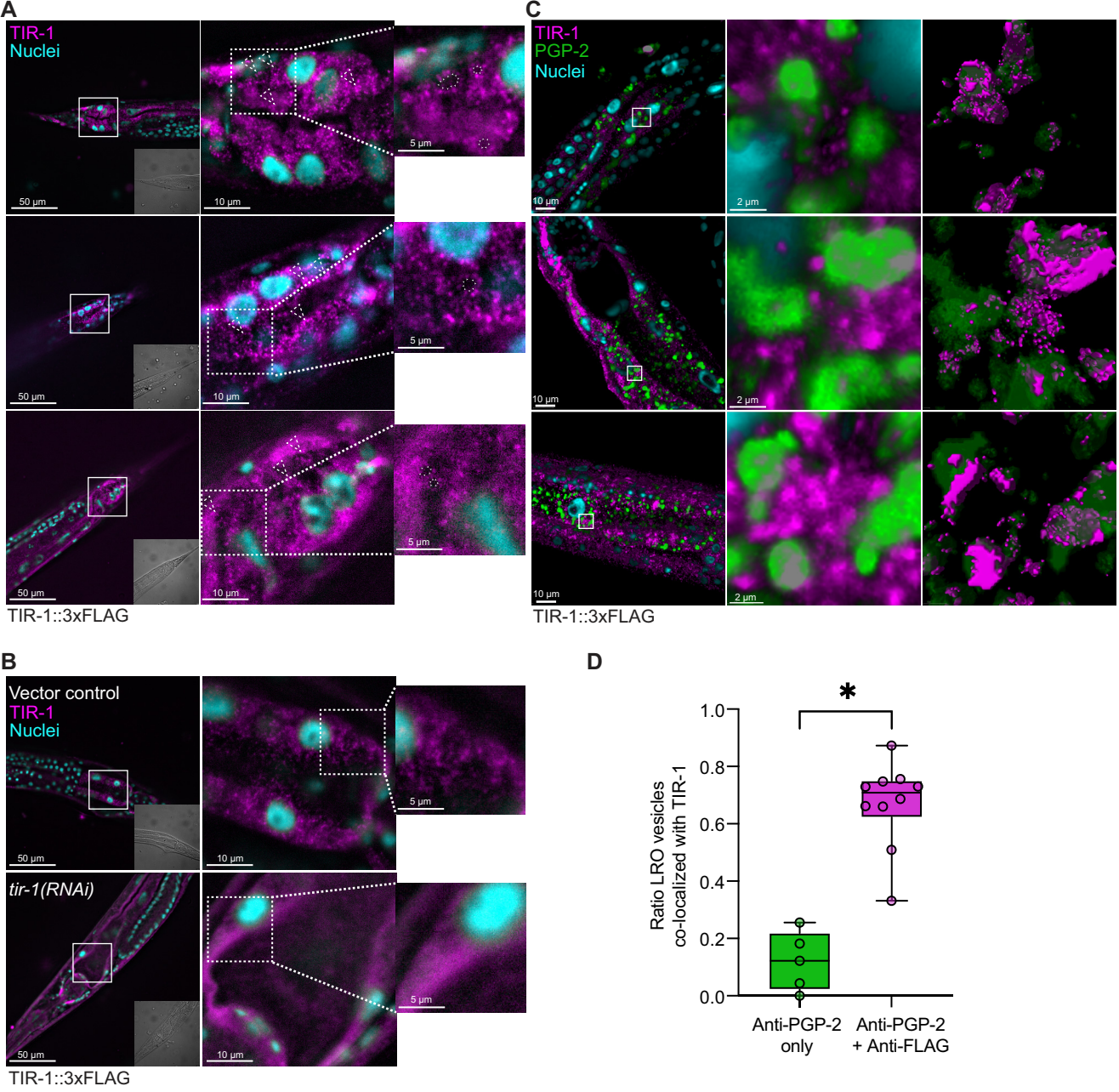
A
TIR-1
Nuclei
50 µm
10 µm
5 µm
TIR-1::3xFLAG
C
TIR-1
PGP-2
Nuclei
10 µm
2 µm
TIR-1::3xFLAG
B
Vector control
TIR-1
Nuclei
tir-1(RNAi)
50 µm
10 µm
5 µm
TIR-1::3xFLAG
D
*
Ratio LRO vesicles co-localized with TIR-1
1.0
0.8
0.6
0.4
0.2
0.0
Anti-PGP-2 only
Anti-PGP-2 + Anti-FLAG

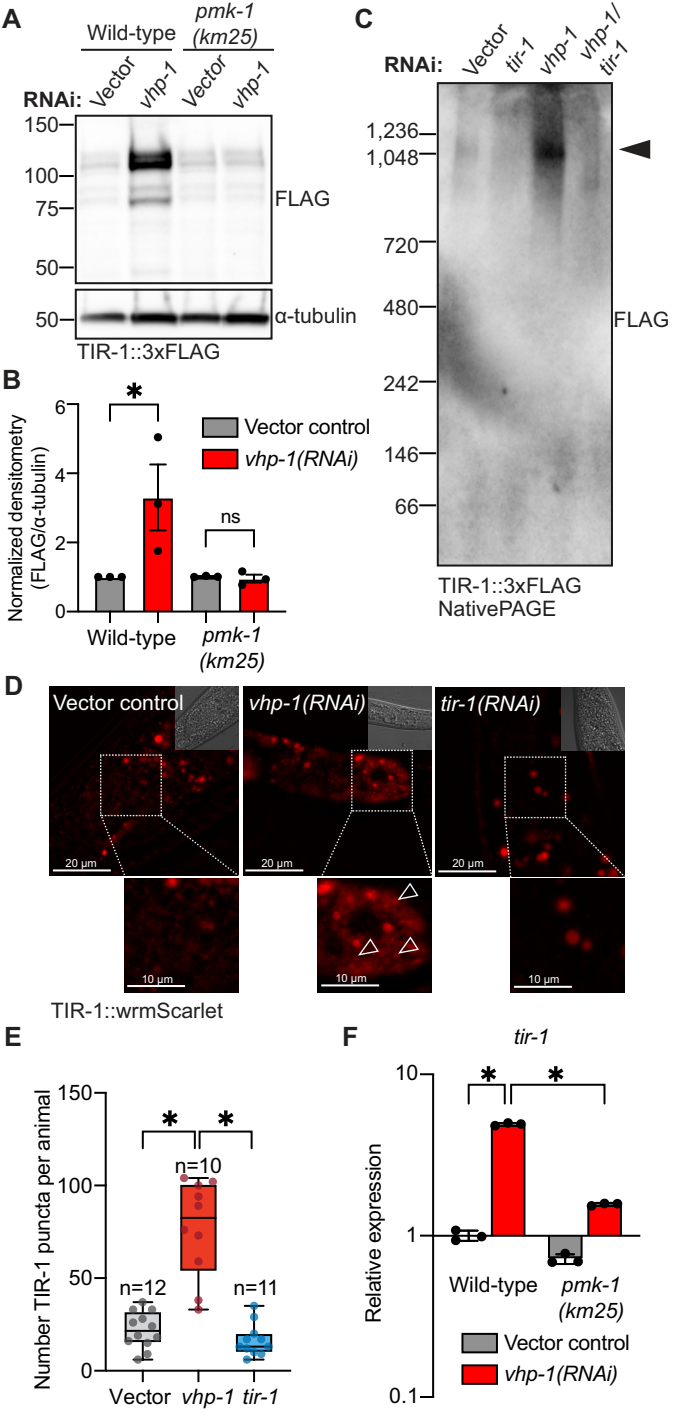
A
Wild-type
pmk-1 (km25)
RNAi:
Vector
vhp-1
Vector
vhp-1
150
100
75
50
FLAG
50
α-tubulin
TIR-1::3xFLAG
B
Normalized densitometry (FLAG/α-tubulin)
6
4
2
0
*
ns
Vector control
vhp-1(RNAi)
Wild-type
pmk-1 (km25)
C
RNAi:
Vector
tir-1
vhp-1
vhp-1/ tir-1
1,236
1,048
720
480
242
146
66
FLAG
TIR-1::3xFLAG NativePAGE
D
Vector control
vhp-1(RNAi)
tir-1(RNAi)
20 µm
10 µm
TIR-1::wrmScarlet
E
Number TIR-1 puncta per animal
150
100
50
0
*
*
n=12
n=10
n=11
Vector
vhp-1
tir-1
F
tir-1
Relative expression
10
1
0.1
*
*
Wild-type
pmk-1 (km25)
Vector control
vhp-1(RNAi)

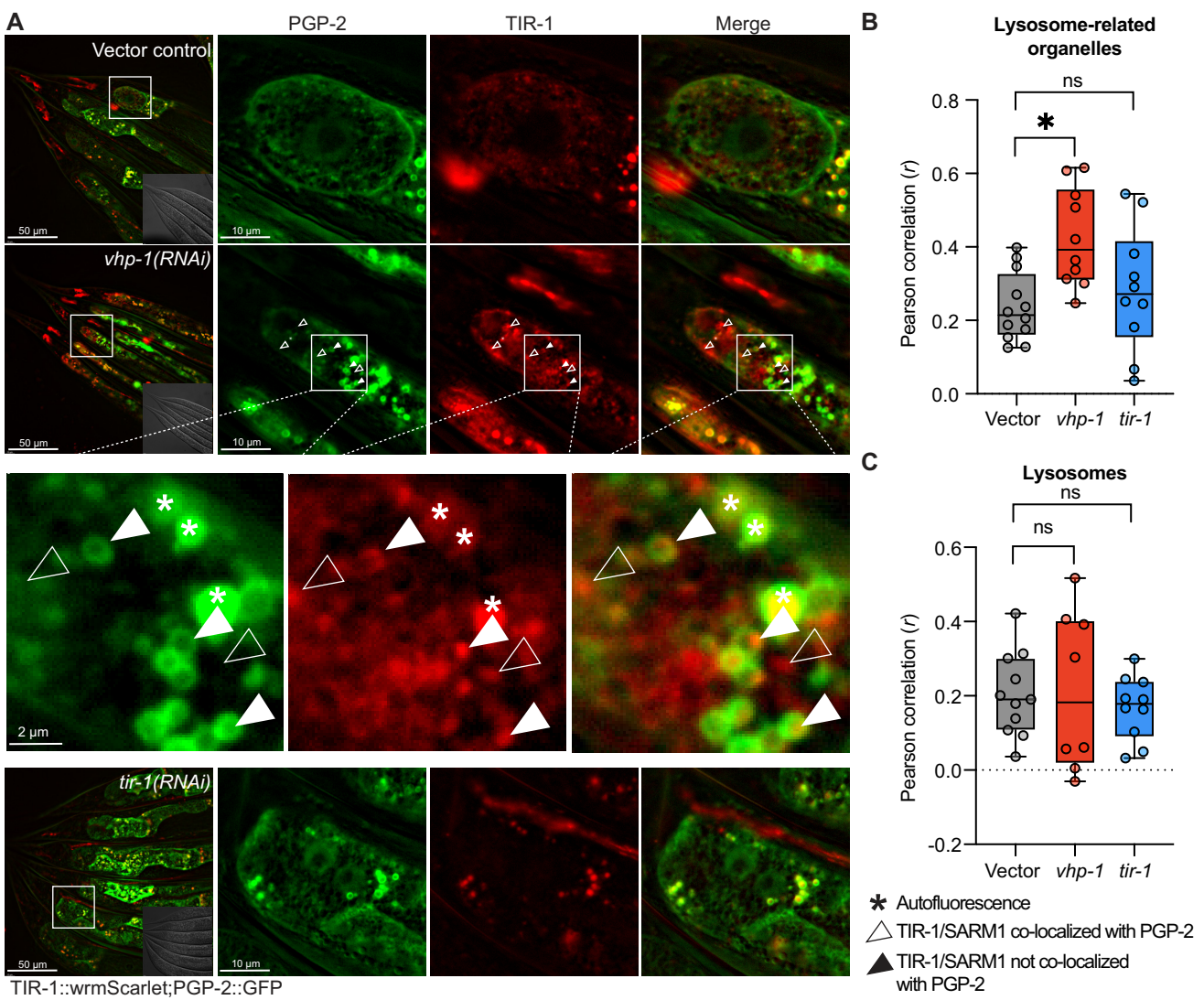
A
PGP-2
TIR-1
Merge
Vector control
vhp-1(RNAi)
tir-1(RNAi)
50 µm
10 µm
2 µm
TIR-1::wrmScarlet;PGP-2::GFP
B
Lysosome-related organelles
ns
*
Pearson correlation (r)
0.8
0.6
0.4
0.2
0.0
Vector
vhp-1
tir-1
C
Lysosomes
ns
ns
0.6
0.4
0.2
0.0
-0.2
Pearson correlation (r)
Vector
vhp-1
tir-1
* Autofluorescence
TIR-1/SARM1 co-localized with PGP-2
TIR-1/SARM1 not co-localized with PGP-2

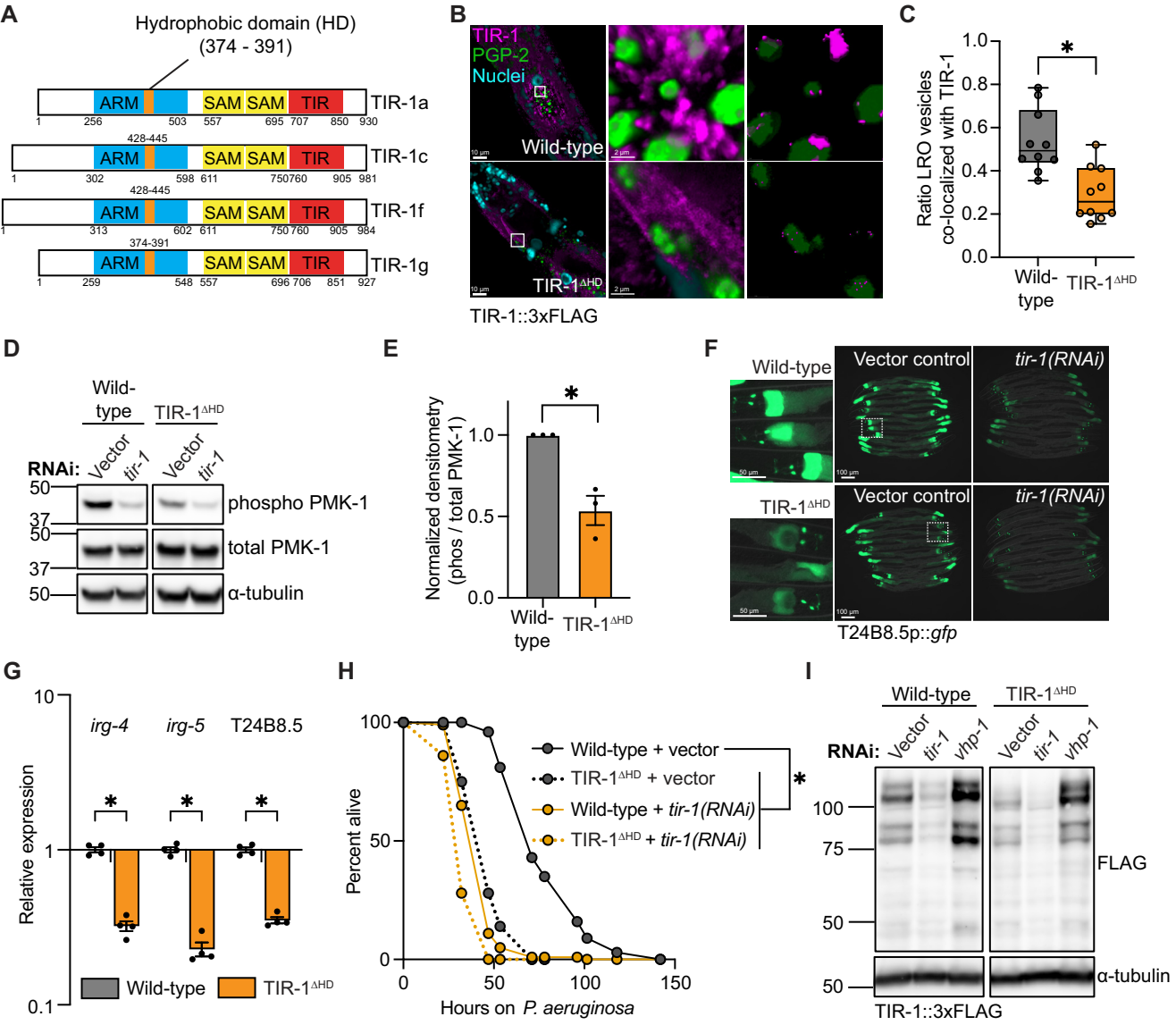
A
Hydrophobic domain (HD)
(374 - 391)
ARM
SAM
SAM
TIR
TIR-1a
1
256
503
557
695
707
850
930
428-445
TIR-1c
302
598
611
750
760
905
981
TIR-1f
313
602
984
374-391
TIR-1g
259
548
696
706
851
927
B
TIR-1
PGP-2
Nuclei
Wild-type
TIR-1ΔHD
TIR-1::3xFLAG
C
Ratio LRO vesicles co-localized with TIR-1
Wild-type
TIR-1ΔHD
D
Wild-type
TIR-1ΔHD
RNAi:
Vector
tir-1
phospho PMK-1
total PMK-1
α-tubulin
E
Normalized densitometry (phos / total PMK-1)
Wild-type
TIR-1ΔHD
F
Wild-type
Vector control
tir-1(RNAi)
TIR-1ΔHD
T24B8.5p::gfp
G
irg-4
irg-5
T24B8.5
Relative expression
Wild-type
TIR-1ΔHD
H
Percent alive
Hours on P. aeruginosa
Wild-type + vector
TIR-1ΔHD + vector
Wild-type + tir-1(RNAi)
TIR-1ΔHD + tir-1(RNAi)
I
Wild-type
TIR-1ΔHD
RNAi:
Vector
tir-1
vhp-1
FLAG
α-tubulin
TIR-1::3xFLAG

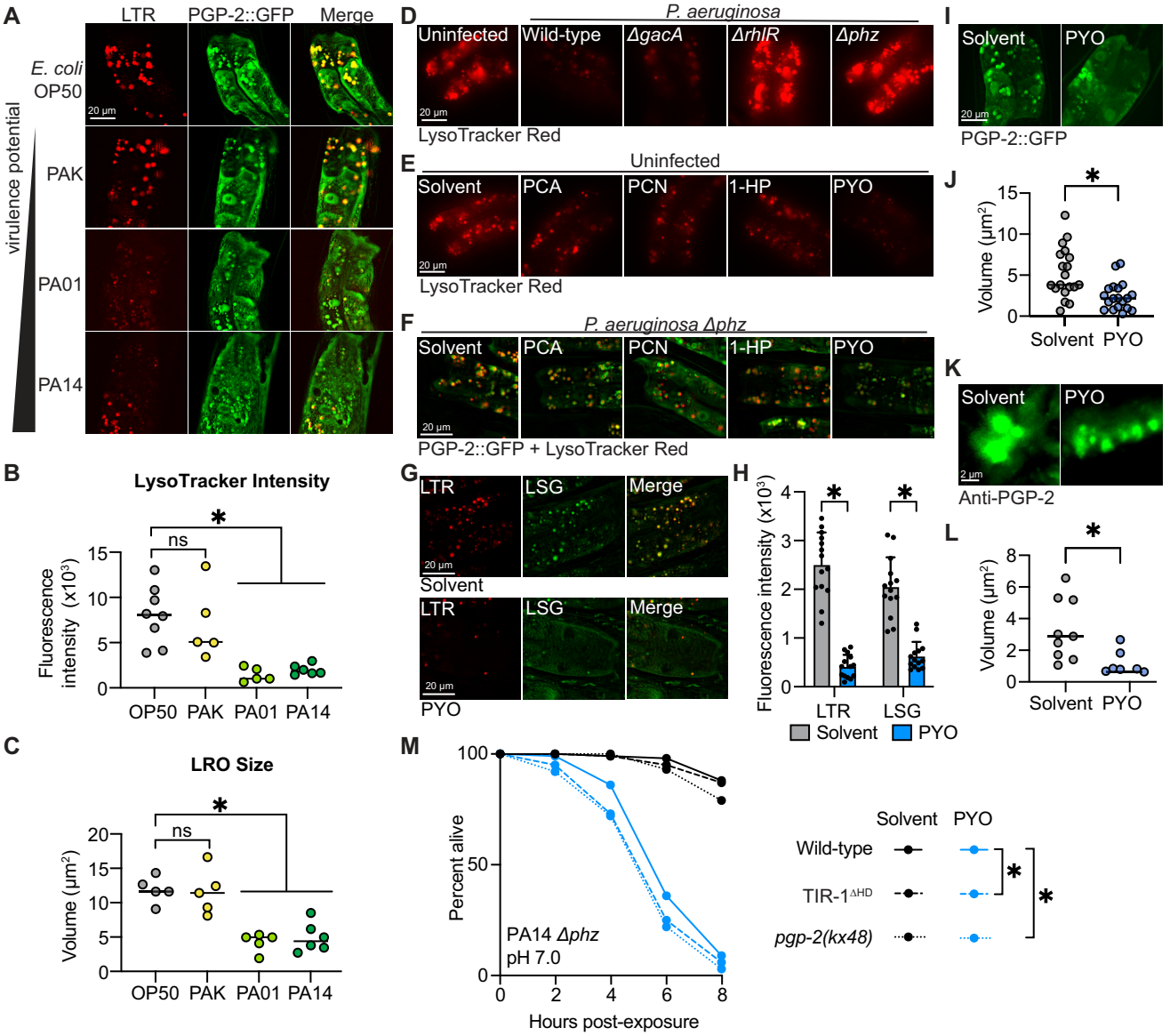
A
LTR
PGP-2::GFP
Merge
E. coli OP50
PAK
PA01
PA14
virulence potential
20 µm
B
LysoTracker Intensity
Fluorescence intensity (x10³)
ns
*
OP50
PAK
PA01
PA14
C
LRO Size
Volume (µm²)
ns
*
D
P. aeruginosa
Uninfected
Wild-type
ΔgacA
ΔrhlR
Δphz
LysoTracker Red
E
Uninfected
Solvent
PCA
PCN
1-HP
PYO
LysoTracker Red
F
P. aeruginosa Δphz
Solvent
PCA
PCN
1-HP
PYO
PGP-2::GFP + LysoTracker Red
G
LTR
LSG
Merge
Solvent
PYO
H
Fluorescence intensity (x10³)
LTR
LSG
Solvent
PYO
I
Solvent
PYO
PGP-2::GFP
J
Volume (µm²)
Solvent
PYO
K
Solvent
PYO
2 µm
Anti-PGP-2
L
Volume (µm²)
Solvent
PYO
M
Percent alive
Hours post-exposure
PA14 Δphz
pH 7.0
Solvent
PYO
Wild-type
TIR-1ΔHD
pgp-2(kx48)

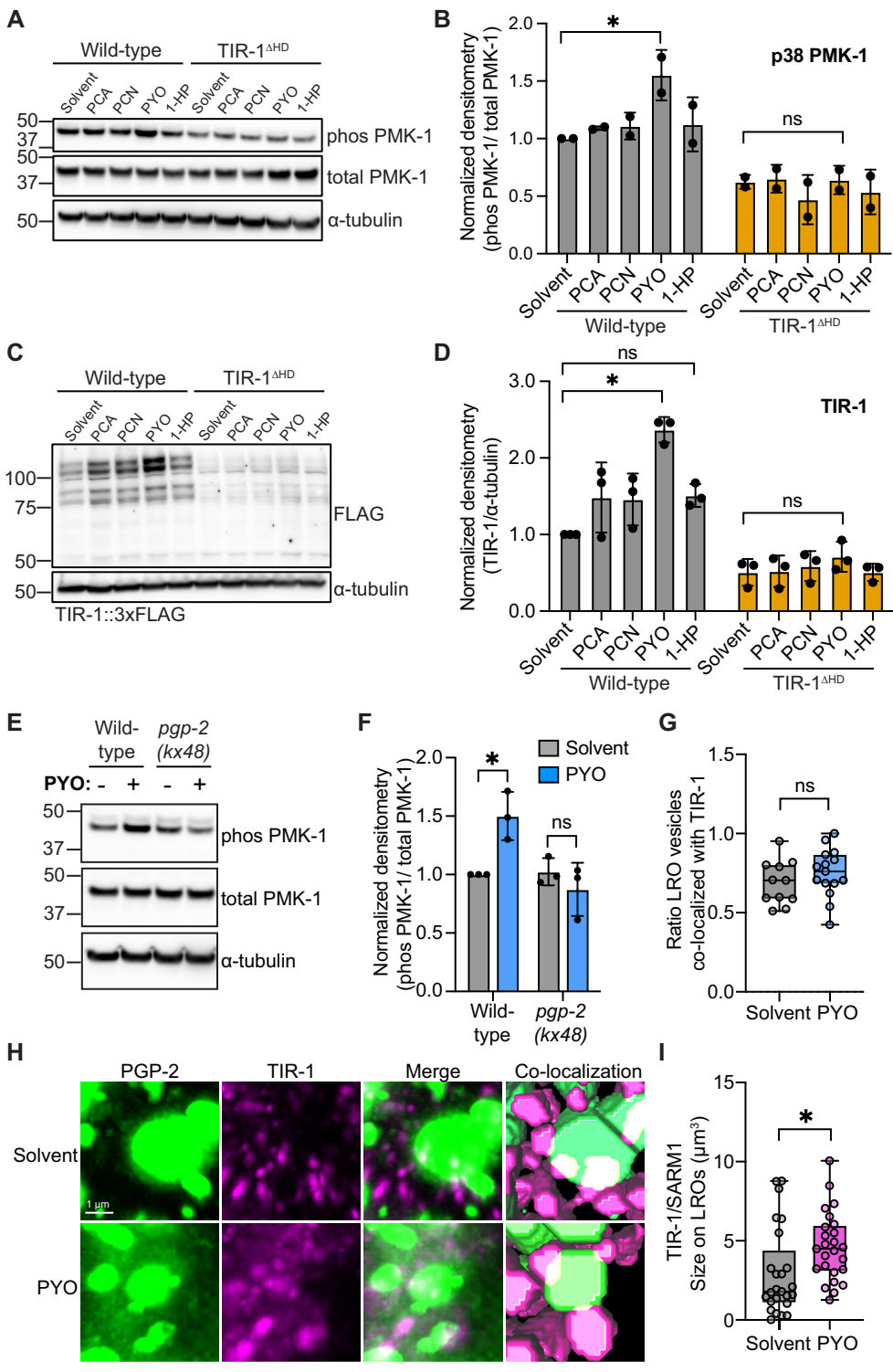
A
Wild-type
TIR-1ΔHD
Solvent
PCA
PCN
PYO
1-HP
50
37
phos PMK-1
total PMK-1
α-tubulin
B
p38 PMK-1
Normalized densitometry (phos PMK-1/ total PMK-1)
*
ns
C
FLAG
100
75
TIR-1::3xFLAG
D
TIR-1
Normalized densitometry (TIR-1/α-tubulin)
E
Wild-type
pgp-2 (kx48)
PYO: - + - +
F
Solvent
PYO
G
Ratio LRO vesicles co-localized with TIR-1
H
PGP-2
TIR-1
Merge
Co-localization
1 µm
I
TIR-1/SARM1 Size on LROs (µm³)

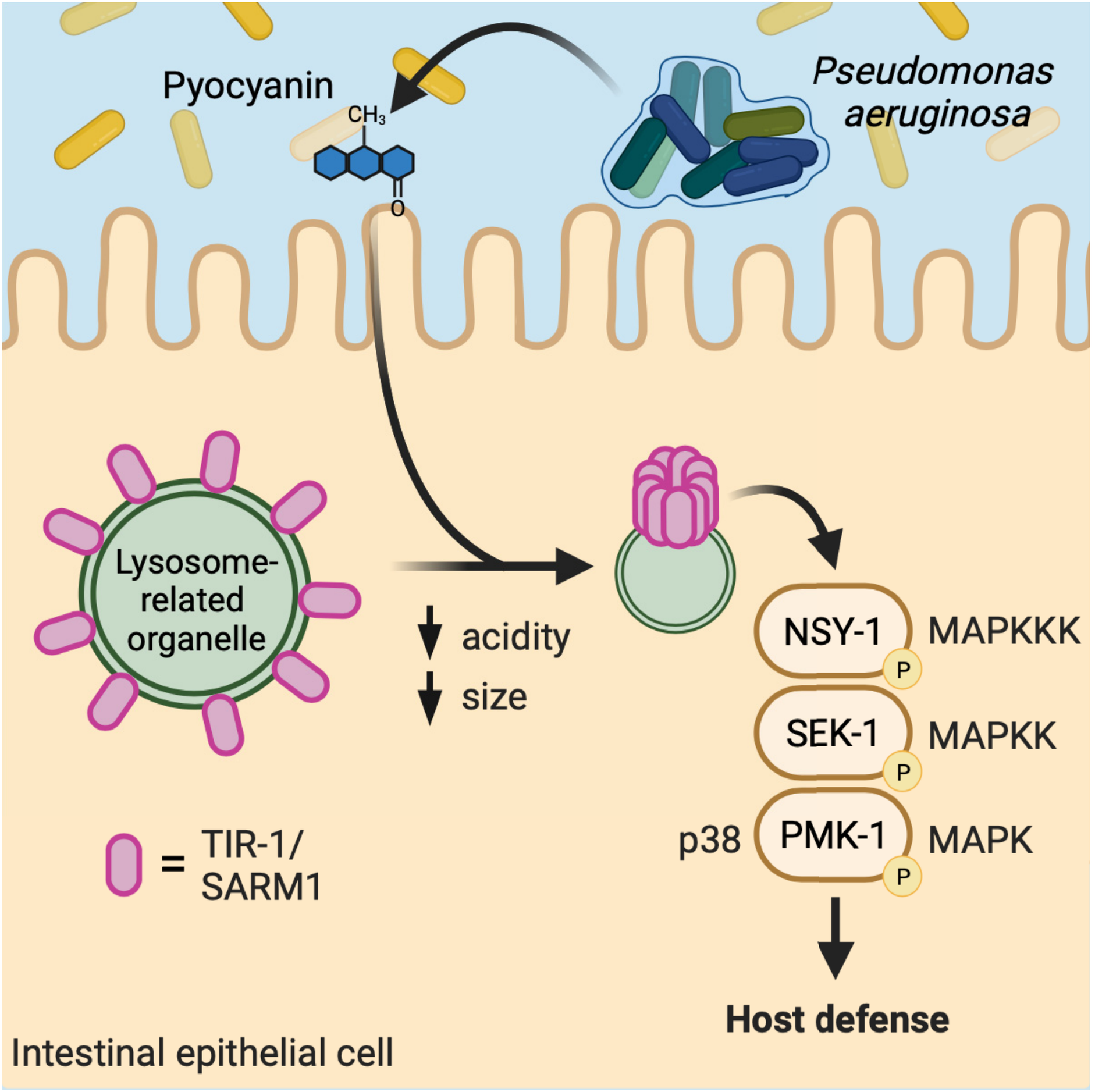
Pyocyanin
CH3
O
Pseudomonas aeruginosa
Lysosome-related organelle
acidity
size
NSY-1
MAPKKK
P
SEK-1
MAPKK
P
p38
PMK-1
MAPK
P
= TIR-1/ SARM1
Host defense
Intestinal epithelial cell

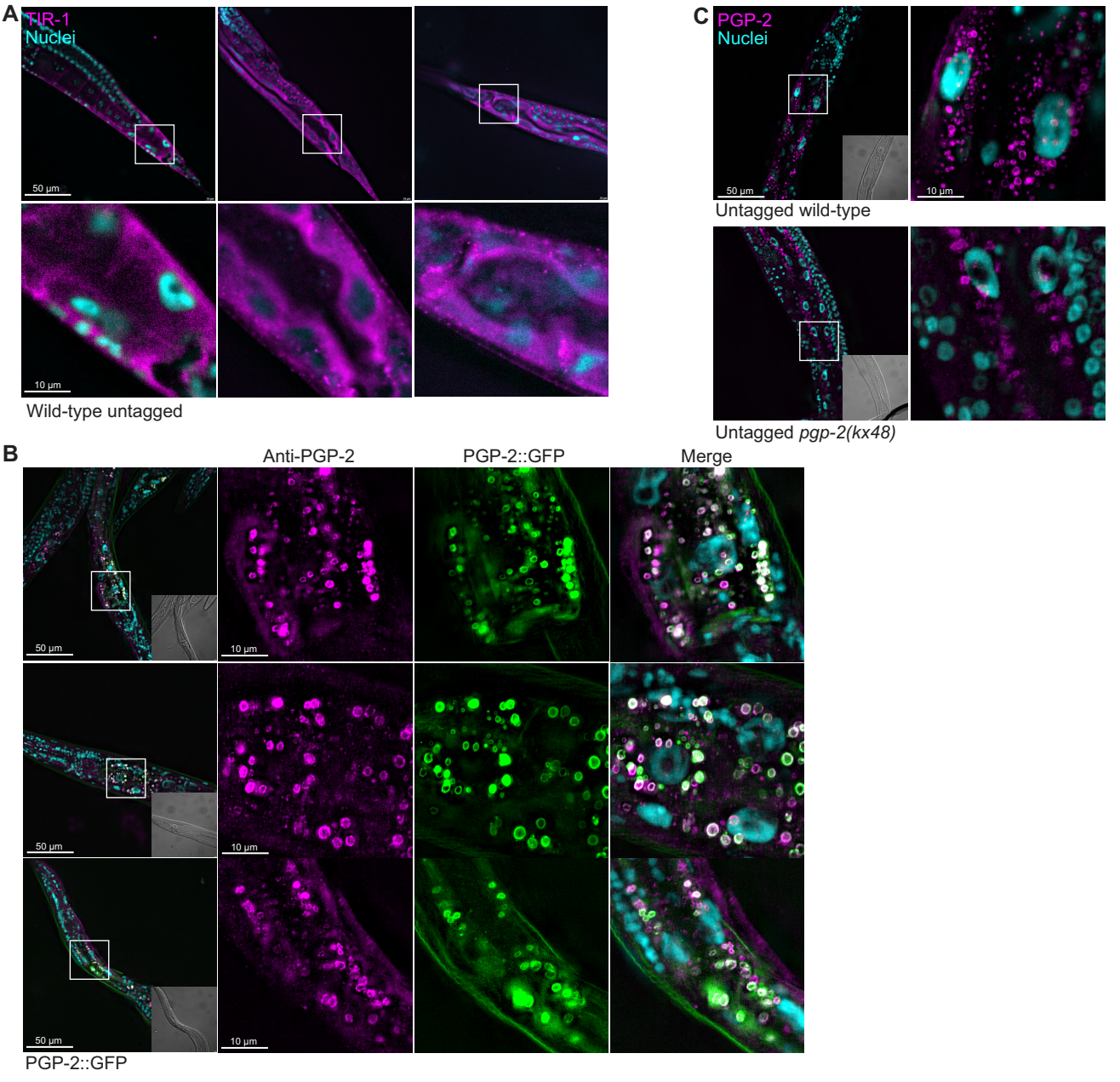
A
TIR-1
Nuclei
50 µm
10 µm
Wild-type untagged
C
PGP-2
Nuclei
50 µm
10 µm
Untagged wild-type
Untagged pgp-2(kx48)
B
Anti-PGP-2
PGP-2::GFP
Merge
50 µm
10 µm
PGP-2::GFP

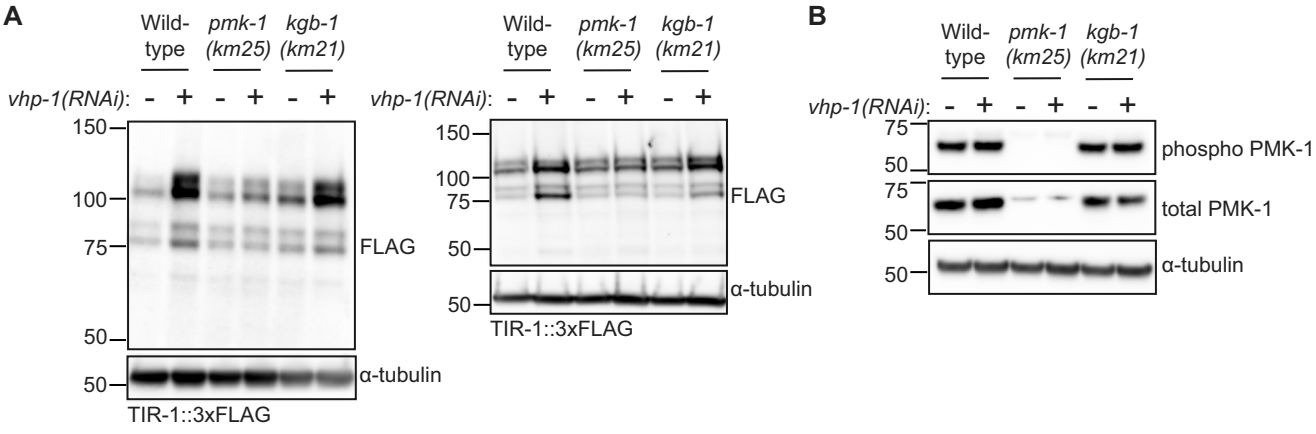
A
Wild-type
pmk-1 (km25)
kgb-1 (km21)
vhp-1(RNAi): - + - + - +
150
100
75
50
FLAG
α-tubulin
TIR-1::3xFLAG
B
phospho PMK-1
total PMK-1

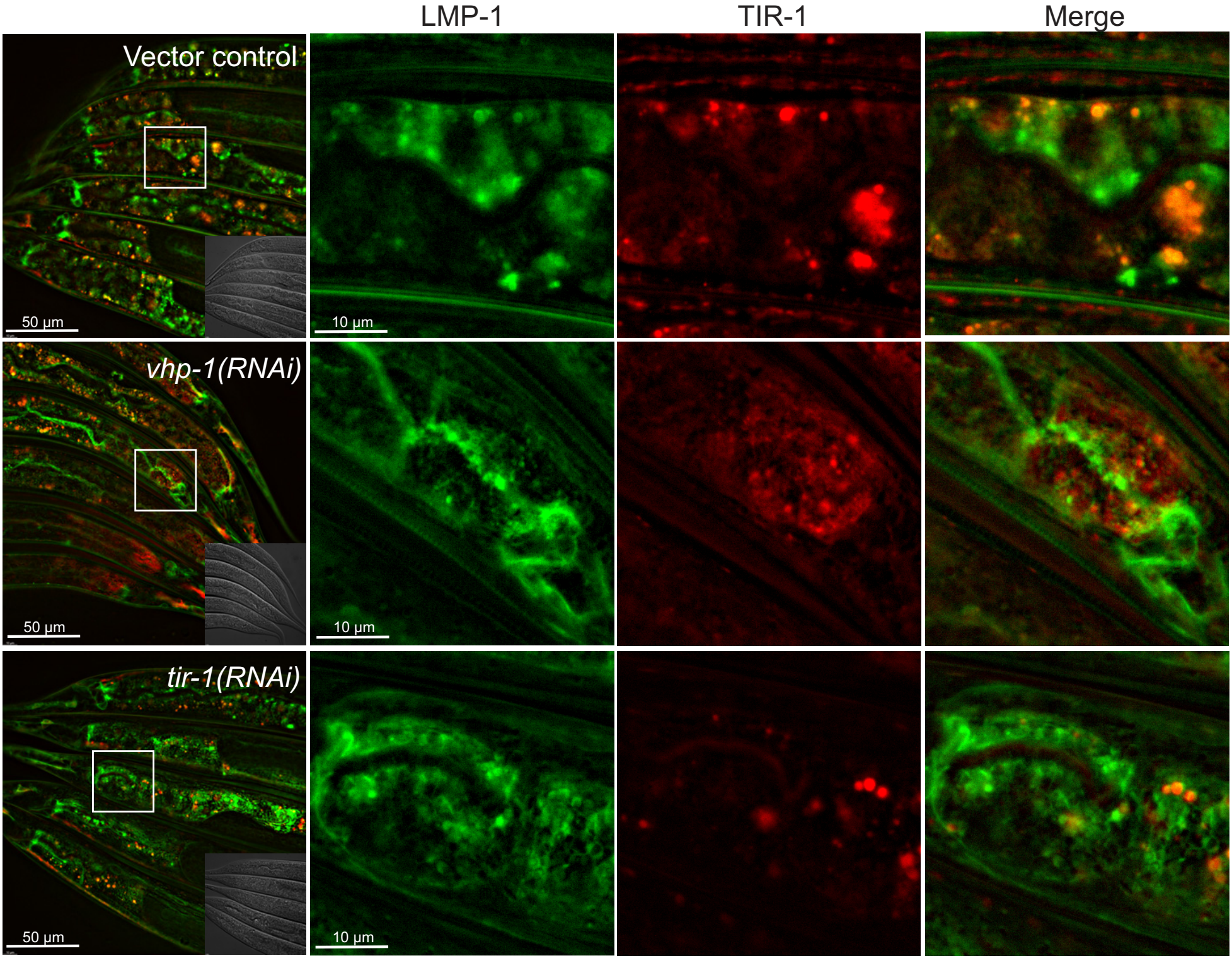

TIR-1::wrmScarlet;LMP-1::GFP

A "DAS" TM-segment prediction

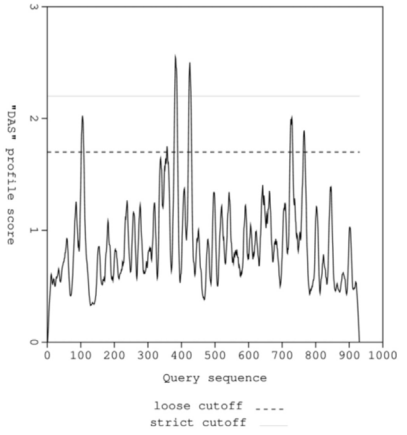

Potential transmembrane segments

Start	Stop	Length	~	Cutoff
102	109	8	~	1.7
357	358	2	~	1.7
378	388	11	~	1.7
380	386	7	~	2.2
421	430	10	~	1.7
423	428	6	~	2.2
724	731	8	~	1.7
763	768	6	~	1.7

B

Phobius prediction

Prediction of UNNAMED

```
ID   UNNAMED
FT   TOPO_DOM      1    373       NON CYTOPLASMIC.
FT   TRANSMEM    374    391
FT   TOPO_DOM    392    930       CYTOPLASMIC.
//
```

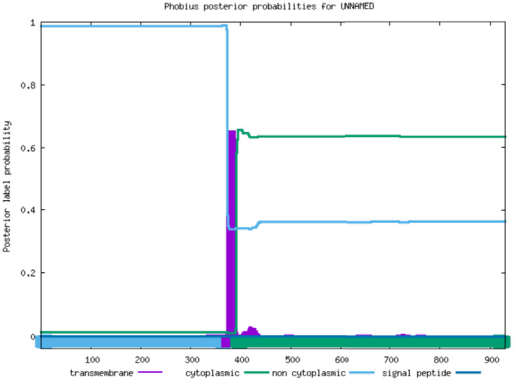

C

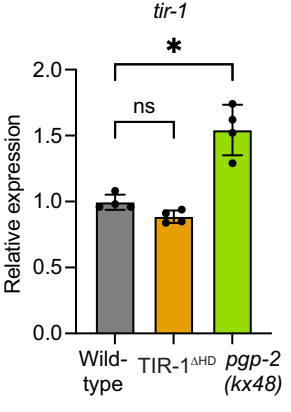

D

TIR-1 isoform	Mol weight (kDa)
a	104.6
b	65.9
c	110.5
d	39
e	91
f	110.9
g	104.3
h	39.3

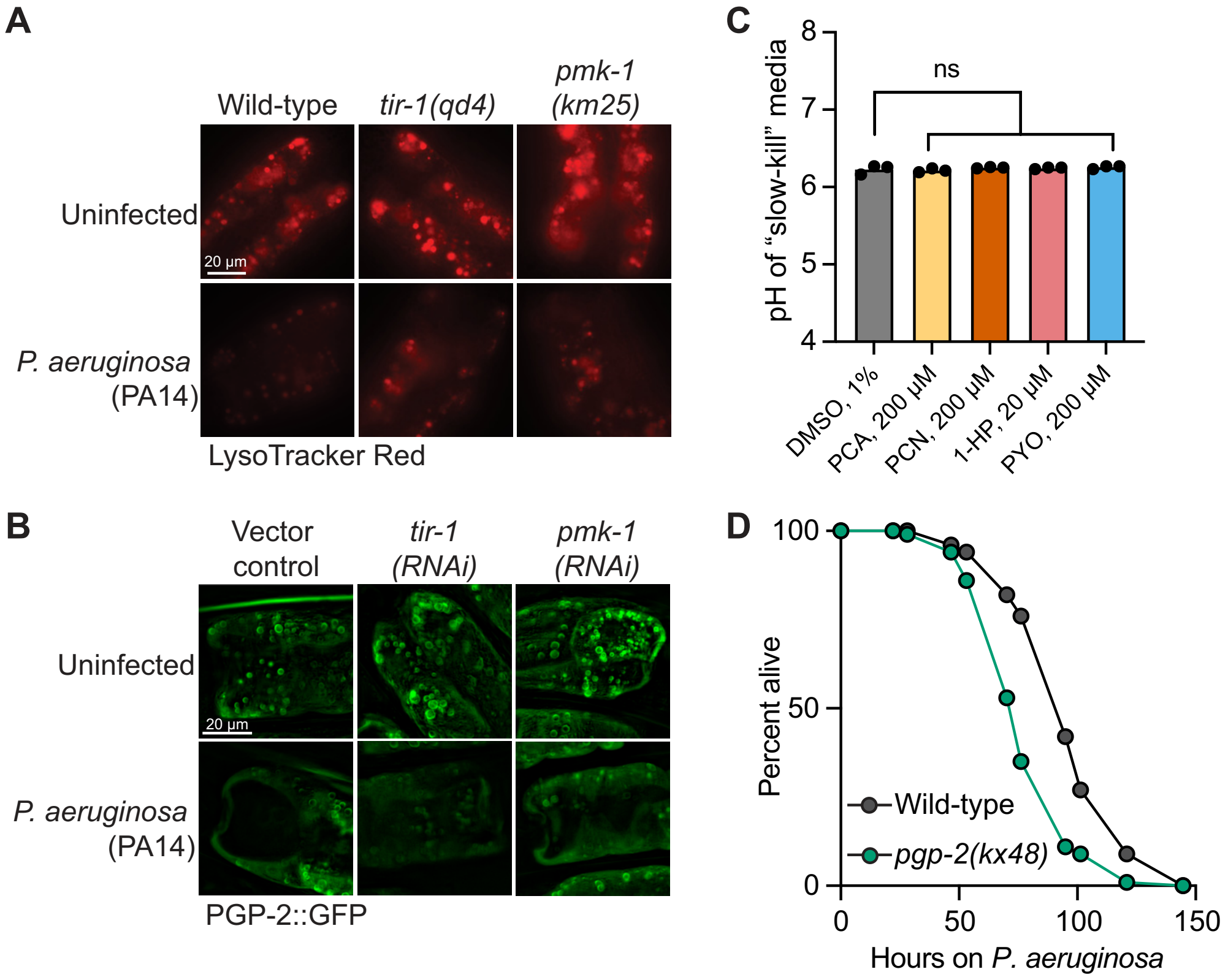
A
Wild-type
tir-1(qd4)
pmk-1 (km25)
Uninfected
P. aeruginosa (PA14)
20 µm
LysoTracker Red
B
Vector control
tir-1 (RNAi)
pmk-1 (RNAi)
Uninfected
P. aeruginosa (PA14)
20 µm
PGP-2::GFP
C
pH of "slow-kill" media
ns
DMSO, 1%
PCA, 200 µM
PCN, 200 µM
1-HP, 20 µM
PYO, 200 µM
D
Percent alive
Hours on P. aeruginosa
Wild-type
pgp-2(kx48)